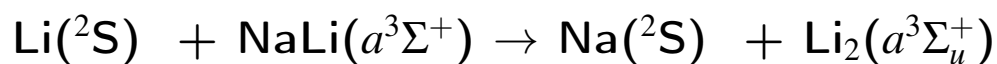


Signatures of Non-universal Quantum Dynamics of Ultracold Chemical Reactions of Polar Alkali-dimer Molecules with Alkali-metal Atoms:



Masato Morita¹, Brian K. Kendrick² Jacek Kłos^{3,4},
Svetlana Kotochigova⁴, Paul Brumer^{1*} and Timur V. Tscherbul^{5*}

¹*Chemical Physics Theory Group, Department of Chemistry, and Center for Quantum Information and Quantum Control, University of Toronto, Toronto, Ontario, M5S 3H6, Canada*

²*Theoretical Division (T-1, MS B221), Los Alamos National Laboratory, Los Alamos, New Mexico 87545, USA,*

³*Joint Quantum Institute, University of Maryland, College Park, Maryland, 20742, USA*

⁴*Department of Physics, Temple University, Philadelphia, PA 19122, USA*

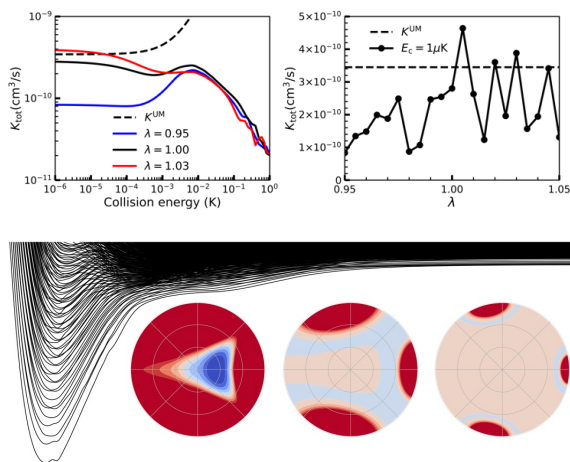
⁵*Department of Physics, University of Nevada, Reno, NV, 89557, USA*

E-mail: paul.brumer@utoronto.ca, ttscherbul@unr.edu

Abstract

Ultracold chemical reactions of weakly bound triplet-state alkali-metal dimer molecules have recently attracted much experimental interest. We perform rigorous quantum scattering calculations with a new *ab initio* potential energy surface to explore the chemical reaction of spin-polarized $\text{NaLi}(a^3\Sigma^+)$ and $\text{Li}(^2\text{S})$ to form $\text{Li}_2(a^3\Sigma_u^+)$ and $\text{Na}(^2\text{S})$. The reaction is exothermic, and proceeds readily at ultralow temperatures. Significantly, we observe strong sensitivity of the total reaction rate to small variations of the three-body part of the Li_2Na interaction at short range, which we attribute to a relatively small number of open $\text{Li}_2(a^3\Sigma_u^+)$ product channels populated in the reaction. This provides the first signature of highly non-universal dynamics seen in rigorous quantum reactive scattering calculations of an ultracold exothermic insertion reaction involving a polar alkali-dimer molecule, opening up the possibility of probing microscopic interactions in atom+molecule collision complexes via ultracold reactive scattering experiments.

TOC Graphic



The study of chemical reactions at low and ultralow temperatures is projected to create major advances in our understanding of chemical reactivity at the most fundamental level.¹⁻⁵ The large deBroglie wavelength of ultracold molecular reactants² combined with the experimenter's ability to prepare them in single well-defined quantum states give rise to pronounced quantum effects, making ultracold chemical reactions an ideal platform for exploring the impact of these fascinating effects on chemical reactivity. Examples include threshold and resonance scattering,^{3,6-8} quantum reflection,⁹⁻¹¹ quantum statistics,^{12,13} and quantum coherent control.^{14,15} In addition, the detection of reaction products and intermediate collision complexes has been experimentally realized,^{16,17} enabling precision tests of long-held statistical theories of chemical dynamics.¹⁸

All chemical reactions studied thus far at low and ultralow temperatures can be classified into abstraction and insertion types.^{19,20} Abstraction reactions, such as $F + H_2 \rightarrow HF + H$ ²¹⁻²³ and $H(D) + H_2 \rightarrow H_2(HD) + D$ ²⁴⁻²⁸ possess an activation barrier, whereas insertion reactions, such as $K + KRb \rightarrow K_2 + Rb$ ^{29,30} and $KRb + KRb \rightarrow K_2 + Rb_2$ ^{18,31} are barrierless and characterized by a deep potential well.³²

Ultracold insertion reactions are generally well described by universal models (UMs),^{13,18,29,33-36} which assume that once the reactants approach each other at close range, they react with unit probability. Exact quantum dynamics calculations showed that the rate of the $K + KRb(X^1\Sigma^+)$ chemical reaction is in excellent agreement with the UM prediction²⁹ and with experiment.³¹ For other insertion chemical reactions, such as $Li + YbLi(X^2\Sigma^+) \rightarrow Li_2(X^1\Sigma_g^+) + Yb$ ^{37,38} and $Li + NaLi(X^1\Sigma^+) \rightarrow Li_2(X^1\Sigma_g^+) + Na$,^{39,40} the calculated deviations from the UM do not exceed 30%.

While UMs are an important tool,^{34,35,41} they do not provide insight into microscopic interactions within the reaction complex,⁶ which is crucial for designing mechanisms to control the reaction dynamics via, e.g., scattering resonances.^{6,42} Similarly, they provide no information about conditions for the validity of UMs, or the parameter dependence of the dynamics. Hence, identifying systems showing significant deviations from universal behavior (*non-universal effects*) is an important goal, which can yield insights into short-range interactions in the reaction complex,

and enable one to tune ultracold chemical reactivity with scattering resonances, a long sought-after goal of ultracold chemistry.^{3,43} Signatures of non-universal effects were observed experimentally in ultracold collisions of Li_2 Feshbach molecules with Li atoms,⁴⁴ and, very recently, in ground rovibrational state molecule-atom and molecule-molecule collisions, such as $\text{K} + \text{NaK}(X^1\Sigma^+)$,⁴⁵ $\text{Na} + \text{NaLi}(a^3\Sigma^+)$ ⁸ and $\text{NaLi} + \text{NaLi}$,⁴⁶ where the observed reaction rate coefficients deviate from UM predictions by several orders of magnitude. The ultracold chemical reaction of polar $\text{NaLi}(a^3\Sigma^+)$ molecules with Li atoms to form the $\text{Li}_2(a^3\Sigma_u^+) + \text{Na}$ products is a natural candidate to search for non-universal effects, as it is energetically allowed [unlike the $\text{Na} + \text{NaLi}(a^3\Sigma^+) \rightarrow \text{Na}_2(a^3\Sigma_u^+) + \text{Li}$ reaction⁷], experimentally feasible,^{8,47,48} and amenable to rigorous theoretical studies due to light reactants.

Non-universal behavior has not yet been seen in rigorous quantum scattering calculations on ultracold chemical reactions of polar alkali dimers. Such behavior has only been predicted for ultracold reactions of *nonpolar* molecules, such as $\text{Li} + \text{Li}_2(a^3\Sigma_u^+)$,^{49,50} $\text{Na} + \text{Na}_2(a^3\Sigma_u^+)$,⁵¹ $\text{K} + \text{K}_2(a^3\Sigma_u^+)$,⁵² and ${}^7\text{Li} + {}^6\text{Li}{}^7\text{Li} \rightarrow {}^7\text{Li}_2 + {}^6\text{Li}$.⁵³ These reactions are unique in that (i) they have a vanishingly small exothermicity, so only a few product states are populated at ultralow temperatures⁵⁴ and (ii) their reactants and products are identical (apart from isotopic substitution). As a result, their zero-temperature rates tend to be below the universal values, on the order of 4.7×10^{-12} cm³/s for the ${}^7\text{Li} + {}^6\text{Li}{}^7\text{Li}$ reaction,⁵⁴ and may not be detectable experimentally. In the most thoroughly studied cases where the reactants and products are identical, it is not even possible to disentangle chemical reactivity from inelastic processes.⁵⁴ By contrast, ultracold chemical reactions probed in recent experiments^{8,48} involve *polar* triplet-state alkali dimers (such as NaLi), and can be exothermic by several hundreds of Kelvin, potentially populating dozens of product rovibrational states.

Here, we show that pronounced non-universal effects can occur in the ultracold insertion reaction of spin-polarized triplet NaLi molecules and Li atoms, $\text{Li}(^2S) + \text{NaLi}(a^3\Sigma^+, v=0, j=0) \rightarrow \text{Li}_2(a^3\Sigma_u^+, v', j') + \text{Na}(^2S)$, significantly extending the range of systems displaying non-universal behavior. We use rigorous quantum scattering calculations based on our *ab initio* interaction

potentials to map out the dependence of the reaction rates on the incident collision energy. Our calculations show that the reaction occurs at a high rate, and hence it can be detected experimentally in an ultracold spin-polarized Li + NaLi mixture. Further, *the total reaction rate is sensitive to small variations of the short-range part of the interaction potential even after summing over all state-to-state reaction rates, and can deviate by a factor of $\simeq 4$ from the UM prediction*, representing the first rigorous theoretical demonstration of non-universal behavior in an ultracold insertion reaction involving a polar molecule. (Note that the non-universal behavior recently observed in ultracold K + NaK, Na + NaLi, and NaLi + NaLi collisions^{8,45,46} is not yet amenable to rigorous quantum scattering calculations due to the large density of rovibrational states of the reactants, non-adiabatic effects, and external fields present in these experiments). We attribute this highly non-universal behavior to a relatively low density of resonance states in this reaction and a limited number of open product channels compared to the chemical reactions explored previously,^{29,37–40} which displayed close to universal behavior. Our results suggest that non-universal effects can be experimentally observed in ultracold chemical reactions of spin-polarized triplet-state alkali-metal dimers with alkali-metal atoms. This opens up the prospects of mapping atom-molecule interactions within the reaction complex, and of controlling the reaction dynamics with external fields, motivating further experimental and theoretical research into non-universal ultracold chemistry.

We consider the chemical reaction of $^{23}\text{Na}^6\text{Li}$ molecules in their metastable triplet electronic states $a^3\Sigma^+$, created in recent experiments.⁴⁷ Figure 1 (a) is a schematic of the reaction path of the $\text{Li}(^2\text{S}) + \text{NaLi}(a^3\Sigma^+) \rightarrow \text{Li}_2(a^3\Sigma_u^+) + \text{Na}(^2\text{S})$ reaction. The three-fold spin degeneracy of $\text{NaLi}(a^3\Sigma^+)$ and the two-fold spin degeneracy of $\text{Li}(^2\text{S})$ give rise to two adiabatic potential energy surfaces (PESs) of doublet ($2^2A'$, $S = 1/2$) and quartet ($1^4A'$, $S = 3/2$) symmetries, where S is the total spin of the reaction complex. The PESs are split at short range by a strong spin-exchange interaction. While the high-spin $1^4A'$ PES is the lowest state in the quartet symmetry, the doublet $2^2A'$ is the *first excited state* in the doublet spin symmetry. The ground-state $1^2A'$ PES [not shown in Fig. 1 (a)] correlates with the $\text{Li}(^2\text{S}) + \text{NaLi}(X^1\Sigma^+)$ reactants in their ground electronic

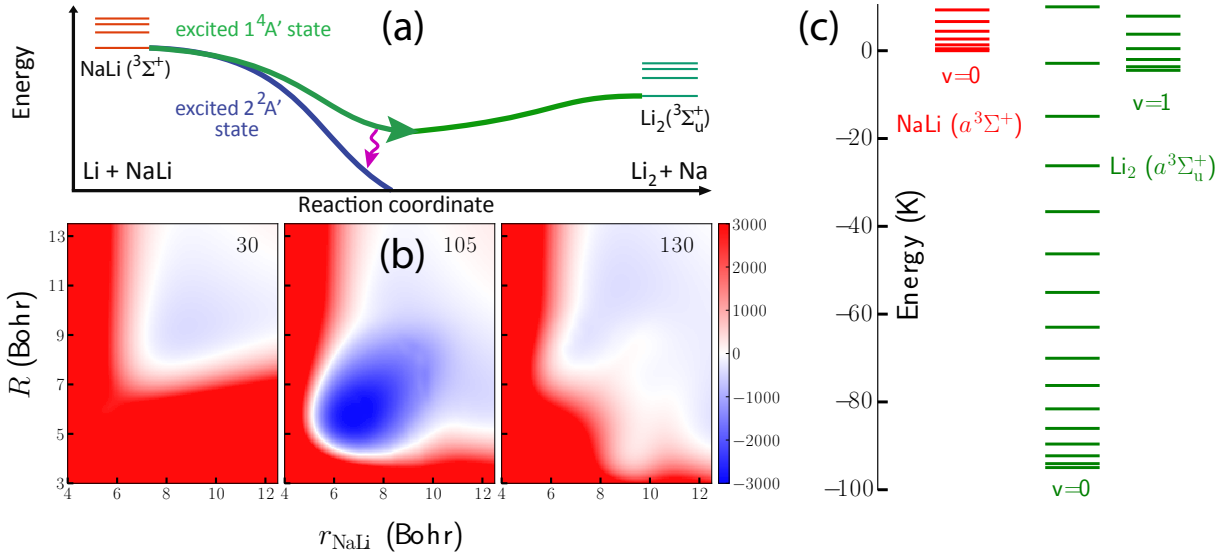


Figure 1: (a) Schematic diagram of the chemical reaction $\text{Li} + \text{NaLi}(a^3\Sigma^+) \rightarrow \text{Li}_2(a^3\Sigma_u^+) + \text{Na}$. The reaction of spin-polarized reactants proceeds via a spin-conserving pathway on the high-spin $1^4A'$ PES (green line) as predicted by the Wigner spin rule. The spin-nonconserving reaction pathway forbidden by the Wigner spin rule (not considered in this work) requires a non-adiabatic transition to the excited $2^2A'$ PES (wavy line). (b) *Ab initio* PES for the $1^4A'$ electronic state of the Li_2Na trimer computed in this work plotted as a function of the Jacobi coordinates (R , r_{NaLi}) at the Jacobi angles $\theta = 30^\circ$ (left), $\theta = 105^\circ$ (middle), and $\theta = 130^\circ$ (right) in the $\text{Li} + \text{NaLi}$ arrangement. (c) Energy diagram for the rovibrational states of the $\text{LiNa}(a^3\Sigma^+)$ reactant and of the $\text{Li}_2(a^3\Sigma_u^+)$ product. The zero of energy corresponds to the energy of the rovibrational ground state of $\text{LiNa}(a^3\Sigma^+, v=0, j=0)$.

states,³⁹ which lie 9629 K below the $\text{Li}(^2\text{S}) + \text{NaLi}(a^3\Sigma^+)$ asymptote of interest here. The ground and the first excited doublet PESs exhibit a conical intersection (CI), which has a pronounced effect on the quantum dynamics of the ultracold chemical reaction of *ground-state* reactants $\text{Li}(^2\text{S}) + \text{NaLi}(X^1\Sigma^+) \rightarrow \text{Li}_2(X^1\Sigma_g^+) + \text{Na}(^2\text{S})$.³⁹

We assume that both $\text{NaLi}(a^3\Sigma^+)$ molecules and Li atoms are prepared in their fully polarized electron spin states prior to the reaction, which is readily achievable experimentally.^{4,8,47} Thereby, the reaction complex is initialized in a state with the total electron spin projection $M_S = \pm 3/2$, which corresponds to $S = 3/2$. Following previous theoretical work,^{49,53,54} we assume the validity of the Wigner spin rule,^{7,43,55–57} which states that S , the total electron spin of the reaction complex, is conserved. This allows us to restrict attention to the quantum dynamics on a single adiabatic

$1^4A'$ PES and neglect the intersystem crossing transitions to the low-spin $1^2A'$ and $2^2A'$ PESs, which exhibit a CI.³⁹ The CI could, in principle, affect the dynamics via intersystem crossing transitions mediated by weak S -nonconserving couplings between the $1^4A'$ PESs and the low-lying PESs due to e.g., the intramolecular spin-spin interaction in NaLi.^{7,58} Model calculations show that such S -nonconserving pathways are typically suppressed by the factor of >10 compared to their S -conserving counterparts in chemical reactions of light atoms and molecules,^{7,36} although infrequent exceptions can occur at certain collision energies and magnetic fields. To rigorously quantify the effect of the doublet PESs and their CI, it is necessary to carry out quantum reactive scattering calculations, which explicitly account for the interactions between the high and low-spin PESs ($1^4A'$, $1^2A'$, and $2^2A'$). At present, this is computationally unfeasible, but progress towards such calculations is currently underway in our laboratories.

We have used the Multi-Reference Configuration Interaction (MRCI) method^{59,60} to calculate the $1^4A'$ PES of the NaLi₂ trimer based on reference wave functions for the two lowest spin-polarized states, $1^4A'$ and $2^4A'$. These reference functions have been obtained from state-averaged Multi-Reference Self-Consistent-Field (MCSCF) calculations.^{61,62} The three valence electrons that describe the NaLi₂ trimer are correlated using an active space composed of 12 orbitals, where nine and three are of A' and A'' symmetry, respectively. The basis sets and effective core and polarization potentials used for Na and Li atoms are described in detail in our recent work,³⁹ which was focused on the energetically lowest spin doublet states $1^2A'$ and $2^2A'$. We performed the electronic structure calculations using the MOLPRO package,⁶³ with further details given in the Supporting Information (SI).⁶⁴ The PES for the $1^4A'$ electronic state of the Li₂Na trimer used in our reactive scattering calculations has the form

$$V_{1^4A'}(r_a, r_b, \alpha) = V_{1^4A'}^{\text{pairwise}}(r_a, r_b, \alpha) + \lambda V_{1^4A'}^{\text{3-body}}(r_a, r_b, \alpha) \quad (1)$$

where r_a and r_b denote the two NaLi bond lengths, α is the bond angle for Li(a)-Na-Li(b), $V_{1^4A'}^{\text{pairwise}}(r_a, r_b, \alpha)$ is the three atom pairwise (two-body) potential obtained by adding together

the spectroscopically accurate $\text{NaLi}(a^3\Sigma^+)$ and $\text{Li}_2(a^3\Sigma_u^+)$ dimer potentials from Refs.^{7,65} and $V_{1^4A'}^{3\text{-body}}(r_a, r_b, \alpha)$ is the non-additive three-body contribution.⁶⁴ The scaling parameter λ is used below to explore the sensitivity of our results to small variations in the non-additive three-body part of the PES. Unless stated otherwise, we assume $\lambda = 1$.

Figure 1(b) shows contour plots of our *ab initio* Li_2Na PES as a function of the Jacobi coordinates (R, r_{NaLi}) for several value of Jacobi angles in the $\text{Li} + \text{NaLi}$ arrangement. The PES is barrierless and the global minimum occurs at $\theta = 105^\circ$ in the $\text{Li} + \text{NaLi}$ arrangement ($R = 5.75 a_0$ and $r = 6.85 a_0$) as shown in the middle panel of Fig. 1(b). The PES depth counted from the minimum of the $\text{Li}_2(a^3\Sigma_u^+)$ product's potential energy curve is 3012 K. The exothermicity of the reaction $\text{Li} + \text{NaLi}(a^3\Sigma^+, v = 0, j = 0) \rightarrow \text{Li}_2(a^3\Sigma_u^+, v' = 0, j' = 0) + \text{Na}$ is ~ 94.9 K (~ 112.0 K) including (excluding) the zero-point energies of the reactants and products. This makes it possible for the reaction to occur at ultralow collision energies. Figure 1(c) shows the internal rovibrational energy levels of the reactants and products calculated from the accurate *ab initio* potential energy curves of $\text{NaLi}(a^3\Sigma^+)$ and $\text{Li}_2(a^3\Sigma_u^+)$.^{7,65} In calculating the energy levels, we neglected the small splittings due to the fine and hyperfine structure of the reactants and products, as done in prior theoretical work on nonpolar alkali dimers.^{49,53,54} This is expected to be a reasonable approximation for fully spin-polarized reactants.⁵⁴ In the limit of zero collision energy, a total of 18 rovibrational states of Li_2 are energetically accessible, including 15 states in the $v' = 0$ manifold ($j' = 0 - 14$) and 3 states in the $v' = 1$ manifold ($j' = 0 - 2$).

To study the quantum dynamics of the ultracold $\text{Li} + \text{NaLi} \rightarrow \text{Li}_2 + \text{Na}$ reaction, we use a rigorous quantum dynamics approach based on the adiabatically adjusting principal-axis frame hyperspherical (APH) coordinates as described in SI.⁶⁴ Figure 2(d) shows the adiabatic eigenvalues $\epsilon_n^{Jpq}(\rho_\xi)$ of the Li_2Na reaction complex calculated using the accurate *ab initio* PES (see SI⁶⁴ for technical details). The corresponding fixed- ρ contour plots of the $1^4A'$ PES as a function of the polar and azimuthal hyperangles are displayed in panels (a)-(c). The entire configuration space can be divided up into three distinct regions. In the short-range region ($\rho = 8 - 15 a_0$) a strongly bound NaLi_2 reaction complex forms, and the different reaction arrangements are strongly coupled. The

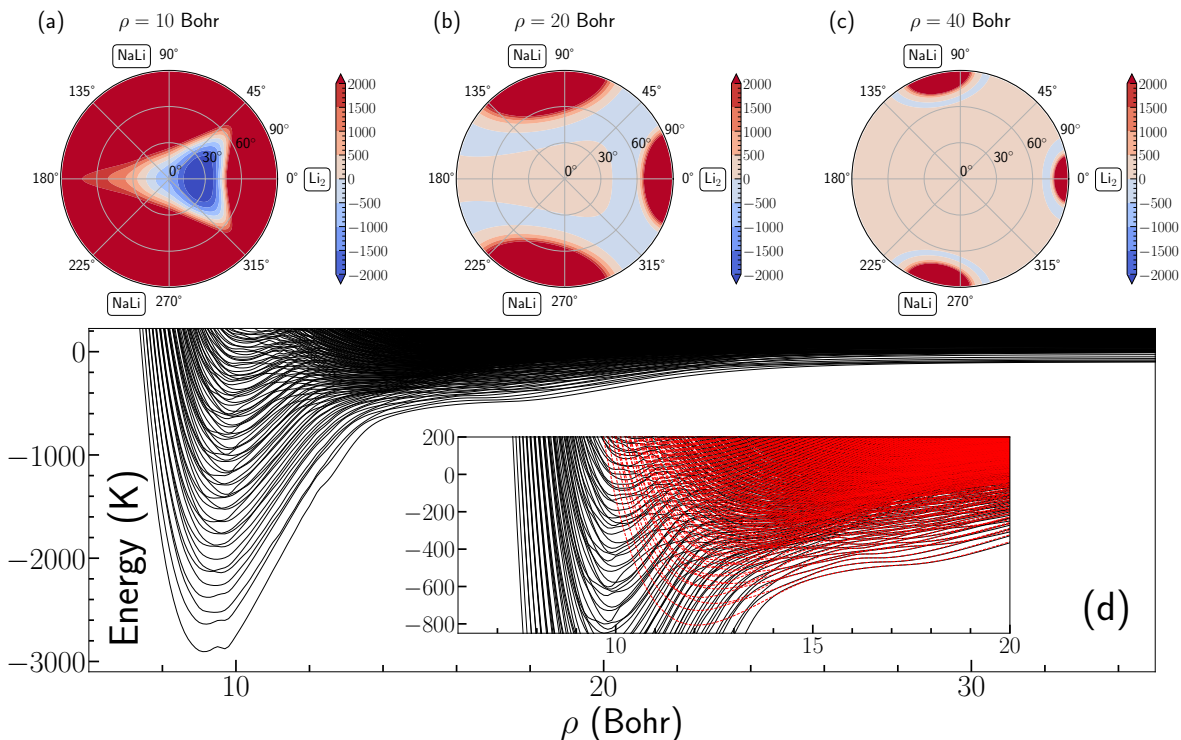


Figure 2: (a)-(c) Stereographic projections of the *ab initio* $1^4A'$ PES of the NaLi₂ trimer for several values of hyperradius (in a_0): $\rho = 10$ (a), $\rho = 20$ (b), and $\rho = 40$ (c). The north pole of the hypersphere is centered at the origin and the zero of energy is chosen at the rovibrational ground state of the NaLi reactant. The region of configuration space accessible at ultralow energies is indicated with blue color. (d) The adiabatic potential curves as a function of ρ for $J = 0^+$ and even exchange symmetry of Li nuclei. The insert shows the adiabatic curves in the vicinity of the reactant threshold. The adiabats calculated without the three-body interaction are shown by the red (light grey) dashed lines.

adiabatic energies range from -3,000 K (near the PES minimum) up to the three-body breakup threshold and above.

In the intermediate region ($\rho = 15 - 40 a_0$) the reactant and product arrangements, while still strongly coupled, begin to separate from one another. As shown in Fig. 2 (c), at $\rho = 20 a_0$ there still exists a large region of configuration space between the reactant and product reaction arrangements (shown in light blue color) where the PES is large and negative. Thus, the reactive scattering wavefunction at $\rho = 20 a_0$ is still substantially delocalized between the reactant and product arrangements. This is because both the reactants and products of the $\text{Li} + \text{NaLi}(a^3\Sigma^+) \rightarrow \text{Li}_2(a^3\Sigma_u^+) + \text{Na}$ chemical reaction are weakly bound (van der Waals, vdW) molecules held together

by long-range dispersion forces, with binding energies not exceeding 300 K.^{66,67} *This makes the vdW chemical reaction studied here significantly different from those of covalently bound molecules such as $\text{Li} + \text{NaLi}(X^1\Sigma^+) \rightarrow \text{Li}_2(X^1\Sigma_g^+) + \text{Na}$,*^{39,40} where the separation of the reactant and product arrangements is essentially complete at much smaller $\rho \simeq 10 - 15 a_0$. This persistence of reactive (inter-arrangement) couplings up to a large ρ is due to the proximity to the three-body breakup threshold, and may be considered as a distinctive feature of quantum dynamics of vdW chemical reactions. We note that in three-body recombination reactions, which start above the three-body threshold, such inter-arrangement couplings occur even asymptotically at large ρ .⁶⁸ Ultracold vdW reactions thus occupy an intermediate position between conventional chemical reactions, which take place at very close range ($\rho \leq 15 a_0$), and three-body recombination transitions (or chemical reactions of Feshbach molecules), which occur at very long range ($\rho \geq 100 a_0$).

The value of $\rho = 40 a_0$ marks the beginning of the long-range region, where the entrance and exit reaction arrangements are completely separated on the surface of a hypersphere by a barrier with a height of > 200 K (note that this barrier does not correspond to an actual barrier in the reaction path). In the limit $\rho \rightarrow \infty$, different reaction arrangements become localized at specific hyperangles θ_α , which correspond to the minima of the diatomic molecule's potentials in each arrangement. The adiabatic curves computed without the three-body terms ($\lambda = 0$) are nearly identical to their three-body counterparts already at $\rho \geq 14 a_0$ as shown in the inset of [Figure 2\(d\)](#). The three-body terms dominate at short range due to a conical intersection between the ground and the first excited quartet PESs.^{54,64,69}

[Figure 3\(a\)](#) shows the total rate of the $\text{Li} + \text{NaLi}(a^3\Sigma^+)$ chemical reaction, $K_{\text{tot}} = \sigma_r v$, where σ_r is the total reaction cross section, and $v = \hbar k / \mu$ is the collision velocity, calculated for several values of the scaling parameter λ . The rates approaches a constant value in the s -wave limit of zero collision energy in keeping with the Wigner threshold law ($K_{\text{tot}} \simeq k^{2l}$). Also plotted in [Figure 3\(a\)](#) is the total universal reaction rate calculated as $K^{\text{UM}} = K_0^{\text{UM}} + K_1^{\text{UM}}(E)$, where K_0^{UM} and $K_1^{\text{UM}}(E)$ are the s -wave and p -wave universal rates calculated as described in Refs. [35](#), [41](#). These are evaluated under the assumption that all of the incoming flux is fully absorbed at short

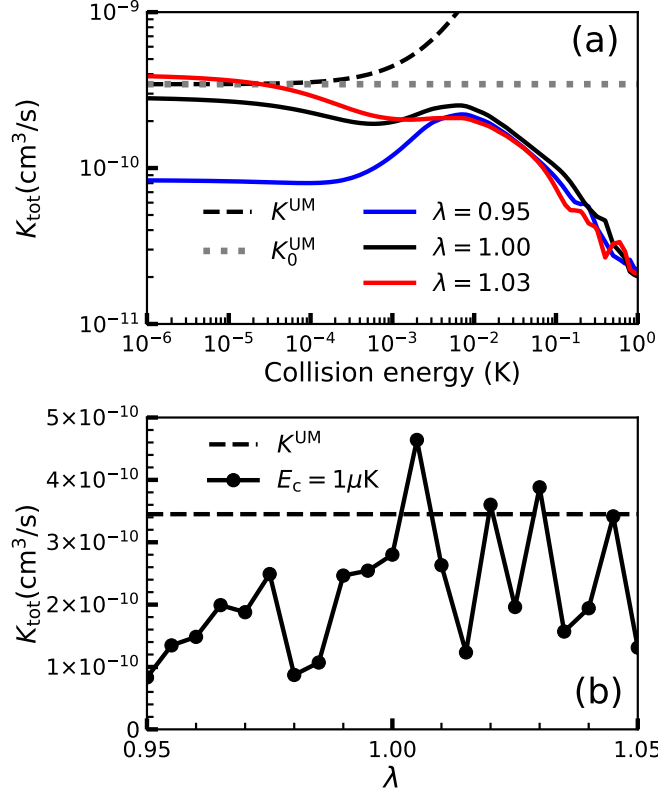


Figure 3: (a) Total rate coefficients for the $\text{Li} + \text{NaLi}(a^3\Sigma^+, v = 0, j = 0) \rightarrow \text{Li}_2(a^3\Sigma_u^+) + \text{Na}$ chemical reaction plotted as functions of collision energy for different values of the PES scaling parameter λ . The universal rate K^{UM} (long dashed line) and its s-wave component K_0^{UM} (short dashed line) are shown. (b) Same as panel (a) at $E = 1 \mu\text{K}$ plotted as a function of λ .

range (loss parameter $y = 1$), which leads to the same universal rate expression, parametrized by the long-range dispersion coefficient C_6 and the reduced mass for the collision, regardless of the details of short-range interactions^{35,41} (see the SI⁶⁴ for more details).

To obtain the universal rates, we calculated the value of $C_6 = 2891$ a.u. for the $\text{Li-NaLi}(a^3\Sigma^+)$ trimer using a high-level spin-restricted coupled-cluster method with single, double, and perturbative triple excitations RCCSD(T) and an aug-cc-pwCVQZ basis set with a bond length of NaLi at $9.0906 a_0$ corresponding to the average internuclear distance of $\text{NaLi}(a^3\Sigma^+, v = 0, j = 0)$.⁶⁴

A striking feature observed in Fig. 3(a) is that the total reaction rate calculated using our exact quantum approach for $\lambda = 0.95$, $K_{\text{tot}} = 8.33 \times 10^{-11} \text{ cm}^3/\text{s}$, is 4.1 times smaller than the universal rate of $K_0^{\text{UM}} = 3.45 \times 10^{-10} \text{ cm}^3/\text{s}$ in the s-wave regime. The reaction rate calculated with $\lambda = 1.03$ is 4.7 times larger than that with $\lambda = 0.95$. This indicates that non-universal effects due to

short-range reflection of the incident scattering flux^{7,8,35} (which appear because not all short-range collisions result in irreversible loss due to, e.g., long-lived complex formation) can play a crucial role in the ultracold chemical reaction $\text{Li} + \text{NaLi}(a^3\Sigma^+) \rightarrow \text{Li}_2(a^3\Sigma_u^+) + \text{Na}$ despite the presence of a deep potential well. This stands in contrast to the behavior observed thus far in quantum scattering calculations on other ultracold atom-molecule insertion reactions.^{29,37,39,40,54} In particular, the chemical reactions of ground-state reactants such as $\text{K} + \text{KRb}(X^1\Sigma^+) \rightarrow \text{K}_2(X^1\Sigma_g^+) + \text{Rb}$,²⁹ $\text{Li} + \text{LiYb}(X^2\Sigma^+) \rightarrow \text{Li}_2(X^1\Sigma_g^+) + \text{Yb}(^1\text{S})$,³⁷ and $\text{Li} + \text{NaLi}(X^1\Sigma^+) \rightarrow \text{Li}_2(X^1\Sigma_g^+) + \text{Na}$ ^{39,40} have deep potential wells and populate a large number of product states, but occur at rates very close (within 30%) to the universal rates. Figure 3(a) shows that the λ dependence of the reaction rate becomes progressively weaker at higher collision energies ($E_c > 10^{-2}$ K) as quantum interference effects are washed out by multiple partial wave contributions.

As shown in Fig. 3(b), the chemical reaction $\text{Li} + \text{NaLi}(a^3\Sigma^+)$ can display both nearly universal as well as highly non-universal dynamics depending on the value of the scaling parameter λ in Eq. (1). The uncertainties in our calculated three-body PES can be estimated at $\pm 5\text{-}10\%$. Thus, while non-universal behavior cannot, at present, be predicted to occur with 100% certainty, the results shown in Fig. 3(b) suggest that its likelihood is much higher than for the previously studied ultracold chemical reactions, such as $\text{Li} + \text{NaLi}(X^1\Sigma^+)$,³⁹ which did not show any significant deviations from universal behavior as a function of λ . Significantly, note that the numerical agreement of the reaction rate with the universal rate does not necessarily mean that the dynamics is well described by the UMs.

To further explore the variation of the rates with the short-range potential, we plot in Fig. 4 the loss rate at the low energy limit using the UM of Ref. 35 as a function of the short-range loss parameter y and the reduced scattering length $s = a/\bar{a}$, where \bar{a} is the mean scattering length given by⁷⁰ $\bar{a} = (2\pi/\Gamma(1/4))^2(2\mu C_6/\hbar^2)^{1/4}$. We observe that for strong loss ($y > 0.8$) it is more likely to observe the rates slightly or below the universal value, as done in this work. In this regime, the small amount of incident flux reflected from the short range without reaction tends to interfere mostly destructively with the incoming flux. The underlying physics is contained in the pole

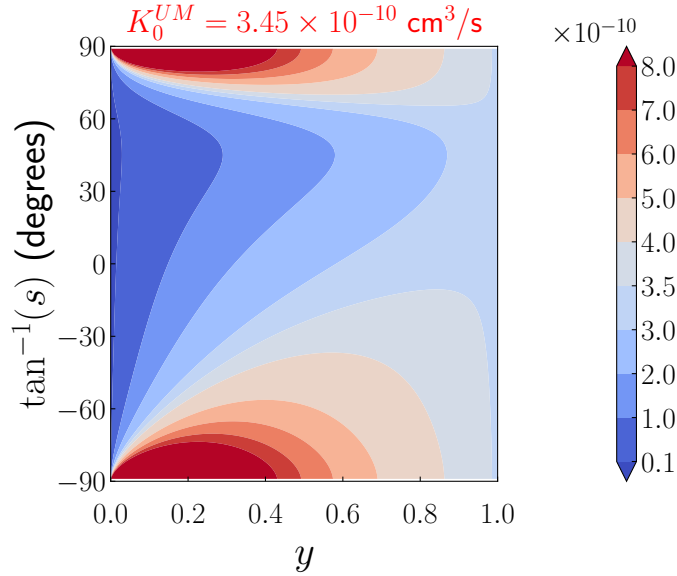


Figure 4: Contour plot of the s -wave loss rate (cm^3/s) calculated using the UM³⁵ as a function of the short-range loss parameter y ($0 \leq y \leq 1$) and the reduced scattering length $s = a/\bar{a}$. In the limit $y \rightarrow 1$, the rate become equal to the universal rate ($K_0^{\text{UM}} = 3.45 \times 10^{-10} \text{ cm}^3/\text{s}$) regardless of the value of s . The loss rate approaches zero as $y \rightarrow 0$.

structure of the complex scattering length (see Eq. (11) of Ref. 35). On the other hand, for $y < 0.5$, observing the rates above the universal value become more and more likely, especially in the case of large $|a|$ (i.e., near a scattering resonance). This is because the amount of reflected flux increases with decreasing y , allowing for a more pronounced quantum interference between the incident and reflected fluxes. As pointed out by Idziaszek and Julienne,³⁵ the quantum interference effects in the UM are counterintuitive, and will be the subject of further study.

To explain the strong variation of the ultracold $\text{Li} + \text{NaLi}(a^3\Sigma^+)$ reaction rate with λ shown in Fig. 3, we recall (see above) that both the reactants and products of this chemical reaction are weakly bound vdW molecules, whose binding energies do not exceed 300 K.⁶⁷ By contrast, the ultracold chemical reactions between alkali-metal and alkaline-earth atoms and molecules studied thus far occur between covalently bound molecules, with binding energies above 1000 K. As a result, the number of open reaction channels populated in these latter reactions (126 for $\text{Li} + \text{NaLi}(^1X)$, 143 for $\text{K} + \text{KRb}$, and 1279 for $\text{Li} + \text{LiYb}$).^{29,38,39} is large compared to the 18 open

channels in the $\text{Li} + \text{NaLi}(a^3\Sigma^+)$ chemical reaction studied here.

The total reaction rate is a sum of the individual state-to-state reaction rates, which fluctuate strongly as a function of λ . These state-to-state fluctuations average out in the total reaction rate, and the degree of averaging depends on the number of contributing state-to-state rates, which is equal to the number of open reaction channels. Because the number of open channels is much smaller for the ultracold $\text{Li} + \text{NaLi}(a^3\Sigma^+)$ vdW reaction, the averaging is not complete, and the total rate fluctuates strongly as a function of λ (see Figs. S3 and S4 of the SI for the details of state-to-state rates). In contrast, the reactions of deeply bound reactants typically populate hundreds of final channels, ensuring nearly complete averaging of the individual state-to-state contributions to the total reaction rate, which then fluctuates only weakly with λ (see, e.g., Fig. 12 of Ref. 39).

This suggests that experimental measurements of state-to-state reaction rates could be used to obtain insight into three-body interactions in triatomic reaction complexes such as NaLi_2 . In particular, if a sufficiently large set of experimental state-to-state rates becomes available, it may be possible to constrain the form of the three-body interaction (the value of λ) uniquely. Such state-to-state measurements have recently been carried out for the ultracold $\text{KRb} + \text{KRb} \rightarrow \text{K}_2 + \text{Rb}_2$ chemical reaction.¹⁸

The near-threshold density of states of the $\text{Li-NaLi}(a^3\Sigma^+)$ trimer can be approximated as $\rho \propto D_e^{3/2} / \sqrt{k_r k_R}$, where D_e is the dissociation energy measured from the minimum of the trimer PES, and k_r and k_R are the harmonic force constants for the NaLi vibrational mode and for the motion along the atom-molecule coordinate R .⁷¹ For the $\text{Li+NaLi}(^4A')$ reaction complex, we estimate the density of states as $\rho = 3.53 \text{ K}^{-1}$, which is 16.7 times lower than that of the $^{40}\text{K}+^{40}\text{K}^{87}\text{Rb}$ trimer ($\rho = 56.6 \text{ K}^{-1}$)⁷¹ (this calculation neglects the hyperfine structure of the reactants).

This is consistent with our calculations (see Fig. 3(b) and Fig. S.3(a) of the SI), which show that state-to-state reaction rates as a function of λ are strongly affected by resonance-like variations. This is because the 5-10% scaling of the three-body term leads to a few hundreds of Kelvin changes in the depth of the PES. It is likely that scattering resonances due to near-threshold bound states are

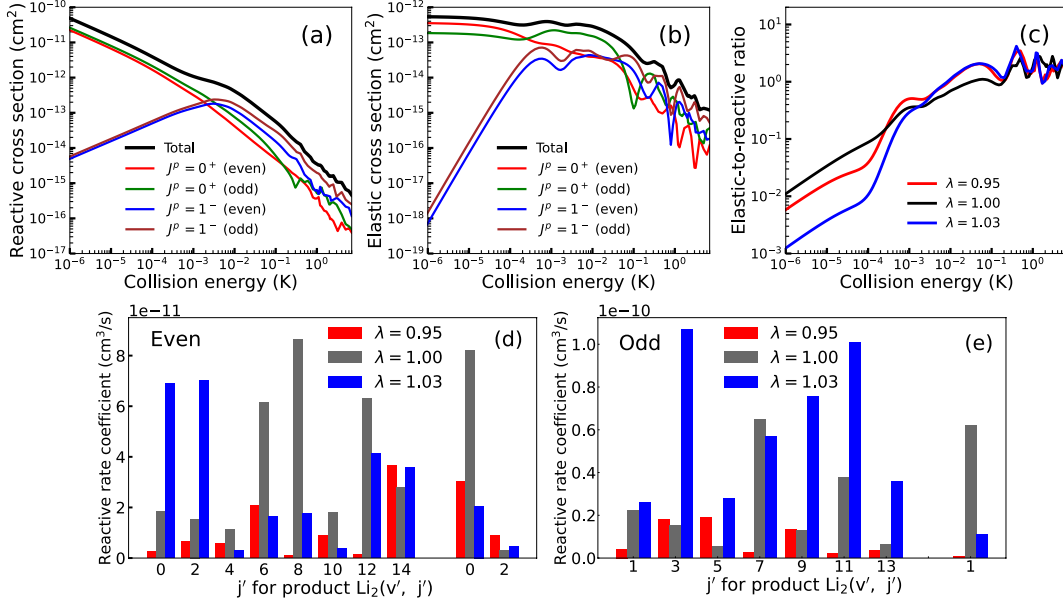


Figure 5: Reactive (a) and elastic (b) cross sections for the ultracold chemical reaction $\text{Li} + \text{NaLi}(v = 0, j = 0) \rightarrow \text{Li}_2 + \text{Na}$ plotted as a function of collision energy for different values of J , parity p and exchange symmetry for $\lambda = 1$. The total integral cross sections (solid black lines) are obtained by summing the cross sections for even and odd ${}^6\text{Li}$ exchange symmetries multiplied by the statistical factors $1/3$ and $2/3$. These factors are the opposite to those used in previous calculations on the ground-state PESs^{37,39,40} because the $X^1\Sigma_g^+$ and $a^3\Sigma_u^+$ electronic states of ${}^6\text{Li}_2$ are even and odd with respect to the exchange of identical Li nuclei. (c) The ratio of elastic to reactive cross sections γ as a function of collision energy for different values of the PES scaling parameter λ . Nascent product state distributions of Li_2 over final rovibrational states (v', j') at $E = 1 \mu\text{K}$ for even (d) and odd (e) j' and three values of λ indicated in the legend. In (d) and (e), the statistical factors for the exchange symmetries are not used.

responsible for the sensitivity, in which case spectroscopic experiments should provide important information on the true value of the three-body interaction. Because the total reaction rate is the sum of 18 independent state-to-state contributions, we expect that it will show variations on much finer λ scales than shown in Fig. 3 (b). While the λ grid interval used in this work is not fine enough to resolve the individual state-to-state oscillations, the potential role of near-threshold resonances in causing these oscillations is an important question to be addressed in future work. In addition, it will be important to explore the sensitivity of state-to-state reaction rates to the anisotropy of the three-body interaction. Finally, the background values of reaction rates could be estimated by averaging the calculated λ -dependent rates over λ .⁷²

In Fig. 5(a) we plot the total integral cross section for the $\text{Li} + \text{NaLi}(a^3\Sigma^+, v=0, j=0)$ reaction (σ_r) as a function of collision energy for several lowest values of J , inversion parity ($p = \pm 1$), and identical Li nuclei exchange symmetry (even/odd). Both even and odd exchange symmetries are seen to contribute to the reactive cross section nearly equally in the s -wave regime ($l = 0$), and the p -wave contributions ($l = 1$) become important at $E > 3$ mK. This behavior is consistent with the Wigner threshold scaling $\sigma_r \simeq E^{l-1/2}$, where l is the orbital angular momentum in the incident channel. The contribution of the even exchange symmetry to the elastic cross section shown in Figure 5(b) is significantly larger than that of the odd symmetry in the s -wave limit, indicating the importance of identical particle permutation symmetry in this reaction. Quantum interference between the Li exchange and non-exchange processes is likely responsible for this behavior as observed in $\text{H} + \text{HD} \rightarrow \text{H} + \text{HD}$ ^{26,64,73} (see also the SI⁶⁴). Above 3 mK, the p -wave ($l = 1$) elastic and reactive cross sections display several broad scattering resonances, whose contribution to the total reaction cross section is largely washed out, making it a smooth function of collision energy all the way up to 100 mK.

The ratio γ of the elastic to reactive cross sections displayed in Fig. 5(c) decreases monotonically in the s -wave limit with decreasing collision energy due to the different threshold scaling of the elastic and inelastic cross sections (see above) regardless of the value of λ . A large elastic-to-inelastic collision ratio ($\gamma \geq 10 - 100$) is an important prerequisite for sympathetic cooling, an experimental technique that relies on momentum-transfer (elastic) collisions of precooled molecules with ultracold atoms to further cool the molecules.⁷⁴⁻⁷⁷ Inelastic collisions and chemical reactions cause trap loss and heating, thereby limiting the efficiency of sympathetic cooling.⁷⁴⁻⁷⁷ The results shown in Fig. 5(c) thus suggest that the chemical reaction $\text{Li} + \text{NaLi}(v=0, j=0) \rightarrow \text{Li}_2 + \text{Na}$ will prevent efficient sympathetic cooling of NaLi molecules via elastic collisions with spin-polarized Li atoms. It's worth noting that the efficient sympathetic cooling observed by Son *et al.*⁴⁸ in a trapped mixture of NaLi molecules with Na atoms would not be adversely affected by the chemical reaction $\text{Na} + \text{NaLi}(a^3\Sigma^+, v=0, j=0) \rightarrow \text{Na}_2(a^3\Sigma_u^+) + \text{Li}$ because it is endothermic, and hence cannot occur at ultralow temperatures.⁷ *Our results thus*

suggest that, in order to achieve efficient sympathetic cooling, the spin-conserving chemical reactions allowed by the Wigner spin rule should be made endothermic via, e.g., a proper choice of atomic collision partners.

Figure 5(d) and (e) show nascent Li_2 product state distributions over the final rovibrational states (v', j') at $E = 1 \mu\text{K}$ for even and odd exchange symmetries. The distributions are highly non-uniform for all λ values and exchange symmetries. The state-to-state reaction rates are highly sensitive to λ due to quantum interference and resonance effects, which, however, are partially averaged out in the total reaction rate (see above).

In summary, motivated by recent experimental advances in measuring collisional properties of ultracold $\text{NaLi}(a^3\Sigma^+)$ molecules with alkali-metal atoms,^{8,48} we have performed accurate *ab initio* and quantum scattering calculations on the prototypical vdW chemical reaction $\text{NaLi}(a^3\Sigma^+) + \text{Li} \rightarrow \text{Li}_2(a^3\Sigma_u^+) + \text{Na}$, which is energetically allowed at ultralow temperatures. We found that the calculated total reaction rate is highly sensitive to tiny changes in the interaction PES (by a factor of $\simeq 4$), which suggests marked deviations from universal behavior.

These results are unprecedented for an ultracold chemical reaction involving a polar molecule. Indeed, all quantum scattering calculations performed thus far^{29,31,38,39} showed that such reactions do not deviate by more than 30% from the universal behavior (see, e.g., Fig. 4 of Ref. 38 and Fig. 7 of Ref. 39). Therefore, the chemical reaction $\text{Li} + \text{NaLi}(a^3\Sigma^+) \rightarrow \text{Li}_2 + \text{Na}$ could be a good candidate for the experimental study of non-universal chemistry in an optically trapped mixture of $\text{NaLi}(a^3\Sigma^+)$ molecules and Li atoms.

A key result of this work is the first observation of strongly non-universal dynamics in an ultracold barrierless insertion reaction involving a polar molecule. The breakdown of universality is remarkable for several reasons. First, it gives us a rare glimpse into a new regime of ultracold chemical dynamics, which cannot be described by simple universal models even at a qualitative level. Second, non-universal dynamics are sensitive to fine details of the underlying PES of the reaction complex. As such, measuring state-resolved reaction rates beyond the universal limit, as done in recent pioneering experiments^{8,46} will enable high-precision characterization

of intermolecular interactions within metastable reaction complexes, a much sought-after goal of ultracold chemistry.^{3,4,43}

Our results also bear significant implications for molecular sympathetic cooling of alkali-dimer molecules by collisions with ultracold atoms in a magnetic trap. The large reaction rates of spin-polarized reactants observed here (see Figure 5(c)) imply that preparing the reactants in their fully spin-polarized initial states will not prevent rapid collisional losses if spin-conserving atom-molecule chemical reactions (such as the $\text{Li} + \text{NaLi}(a^3\Sigma^+)$ reaction explored here) are energetically allowed. This leads to a general design principle for choosing ultracold atom-molecule systems suitable for sympathetic cooling experiments: Avoid spin-conserving chemical reactions by choosing the coolant atom in such a way as to make the reaction endothermic, and hence energetically forbidden at ultralow temperatures.

Supporting Information

See the supporting information associated with this article for details of *ab initio* calculations of the $^4A'$ PES of the Li_2Na trimer and for technical details of quantum reactive scattering calculations.

Acknowledgement

M.M. thanks Dr. Pablo G. Jambrina for useful discussions. This work was supported by the NSF through the CAREER program (PHY-2045681) and by the U.S. Air Force Office for Scientific Research (AFOSR) under Contracts Nos. FA9550-19-1-0312 and FA9550-22-1-0361 to P.B. and T.V.T. J.K. and S.K. acknowledge support from the U.S. AFOSR under Grant No. FA9550-21-1-0153 and the NSF under Grant No. PHY-1908634. B.K.K. acknowledges that part of this work was done under the auspices of the US Department of Energy under Project No. 20170221ER of the Laboratory Directed Research and Development Program at Los Alamos National Laboratory. This work used resources provided by the Los Alamos National Laboratory Institutional Computing Program. Los Alamos National Laboratory is operated by Triad National

Security, LLC, for the National Nuclear Security Administration of the U.S. Department of Energy (contract No. 89233218CNA000001).

Data availability statement

The data that support the findings of this study are available within the article and its supporting information. Data is also available from the authors upon reasonable request.

References

- (1) Carr, L. D.; DeMille, D.; Krems, R. V.; Ye, J. Cold and ultracold molecules: Science, technology and applications. *New J. Phys* **2009**, *11*, 055049.
- (2) Herschbach, D. Molecular collisions, from warm to ultracold. *Faraday Discuss.* **2009**, *142*, 9–23.
- (3) Balakrishnan, N. Perspective: Ultracold molecules and the dawn of cold controlled chemistry. *J. Chem. Phys.* **2016**, *145*, 150901.
- (4) Bohn, J. L.; Rey, A. M.; Ye, J. Cold molecules: Progress in quantum engineering of chemistry and quantum matter. *Science* **2017**, *357*, 1002–1010.
- (5) Liu, Y.; Ni, K.-K. Bimolecular chemistry in the ultracold regime. *Annu. Rev. Phys. Chem.* **2022**, *73*, 73–96.
- (6) Tscherbul, T. V.; Krems, R. V. Tuning bimolecular chemical reactions by electric fields. *Phys. Rev. Lett.* **2015**, *115*, 023201.
- (7) Hermsmeier, R.; Kłos, J.; Kotochigova, S.; Tscherbul, T. V. Quantum spin state selectivity and magnetic tuning of ultracold chemical reactions of triplet alkali-metal dimers with alkali-metal atoms. *Phys. Rev. Lett.* **2021**, *127*, 103402.

- (8) Son, H.; Park, J. J.; Lu, Y.-K.; Jamison, A. O.; Karman, T.; Ketterle, W. Control of reactive collisions by quantum interference. *Science* **2022**, *375*, 1006–1010.
- (9) Orzel, C.; Walhout, M.; Sterr, U.; Julienne, P. S.; Rolston, S. L. Spin polarization and quantum-statistical effects in ultracold ionizing collisions. *Phys. Rev. A* **1999**, *59*, 1926–1935.
- (10) Mody, A.; Haggerty, M.; Doyle, J. M.; Heller, E. J. No-sticking effect and quantum reflection in ultracold collisions. *Phys. Rev. B* **2001**, *64*, 085418.
- (11) Bai, Y.-P.; Li, J.-L.; Wang, G.-R.; Cong, S.-L. Model for investigating quantum reflection and quantum coherence in ultracold molecular collisions. *Phys. Rev. A* **2019**, *100*, 012705.
- (12) Ni, K.-K.; Ospelkaus, S.; Wang, D.; Quéméner, G.; Neyenhuis, B.; de Miranda, M. H. G.; Bohn, J. L.; Ye, J.; Jin, D. S. Dipolar collisions of polar molecules in the quantum regime. *Nature (London)* **2010**, *464*, 1324–1328.
- (13) Quéméner, G.; Julienne, P. S. Ultracold molecules under control! *Chem. Rev.* **2012**, *112*, 4949–5011.
- (14) Devolder, A.; Tscherbil, T. V.; Brumer, P. Coherent control of reactive scattering at low temperatures: Signatures of quantum interference in the differential cross sections for $F + H_2$ and $F + HD$. *Phys. Rev. A* **2020**, *102*, 031303(R).
- (15) Devolder, A.; Brumer, P.; Tscherbil, T. V. Complete quantum coherent control of ultracold molecular collisions. *Phys. Rev. Lett.* **2021**, *126*, 153403.
- (16) Hu, M.-G.; Liu, Y.; Grimes, D. D.; Lin, Y.-W.; Gheorghe, A. H.; Vexiau, R.; Bouloufa-Maafa, N.; Dulieu, O.; Rosenband, T.; Ni, K.-K. Direct observation of bimolecular reactions of ultracold KRb molecules. *Science* **2019**, *366*, 1111–1115.
- (17) Liu, Y.; Hu, M.-G.; Nichols, M. A.; Grimes, D. D.; Karman, T.; Guo, H.; Ni, K.-K. Photoexcitation of long-lived transient intermediates in ultracold reactions. *Nat. Phys.* **2020**, *16*, 1132–1136.

- (18) Liu, Y.; Hu, M.-G.; Nichols, M. A.; Yang, D.; Xie, D.; Guo, H.; Ni, K.-K. Precision test of statistical dynamics with state-to-state ultracold chemistry. *Nature* **2021**, *593*, 379–384.
- (19) Weck, P. F.; Balakrishnan, N. Importance of long-range interactions in chemical reactions at cold and ultracold temperatures. *Int. Rev. Phys. Chem.* **2006**, *25*, 283–311.
- (20) Krems, R. V. *Molecules in electromagnetic fields: from ultracold physics to controlled chemistry*; John Wiley & Sons, Ltd: Hoboken, NJ, 2018.
- (21) Balakrishnan, N.; Dalgarno, A. Chemistry at ultracold temperatures. *Chem. Phys. Lett.* **2001**, *341*, 652–656.
- (22) Tizniti, M.; Le Picard, S. D.; Lique, F.; Berteloite, C.; Canosa, A.; Alexander, M. H.; Sims, I. R. The rate of the F + H₂ reaction at very low temperatures. *Nat. Chem.* **2014**, *6*, 141–145.
- (23) De Fazio, D.; Aquilanti, V.; Cavalli, S. Quantum dynamics and kinetics of the F + H₂ and F + D₂ reactions at low and ultra-low temperatures. *Front. Chem.* **2019**, *7*, 328–328.
- (24) Simbotin, I.; Ghosal, S.; Côté, R. A case study in ultracold reactive scattering: D + H₂. *Phys. Chem. Chem. Phys.* **2011**, *13*, 19148–19155.
- (25) Simbotin, I.; Côté, R. Effect of nuclear spin symmetry in cold and ultracold reactions: D + para/ortho-H₂. *New J. Phys.* **2015**, *17*, 065003.
- (26) Kendrick, B. K.; Hazra, J.; Balakrishnan, N. Geometric phase appears in the ultracold hydrogen exchange reaction. *Phys. Rev. Lett.* **2015**, *115*, 153201.
- (27) Kendrick, B. K. Non-adiabatic quantum reactive scattering calculations for the ultracold hydrogen exchange reaction: H + H₂($v = 4 - 8, j = 0$) → H + H₂(v', j'). *Chem. Phys.* **2018**, *515*, 387–399.
- (28) Kendrick, B. K. Nonadiabatic ultracold quantum reactive scattering of hydrogen with vibrationally excited HD($v = 5 - 9$). *J. Phys. Chem. A* **2019**, *123*, 9919–9933.

- (29) Croft, J. F. E.; Makrides, C.; Li, M.; Petrov, A.; Kendrick, B. K.; Balakrishnan, N.; Kotochigova, S. Universality and chaoticity in ultracold K + KRb chemical reactions. *Nat. Commun.* **2017**, *8*, 15897.
- (30) Croft, J. F. E.; Balakrishnan, N.; Kendrick, B. K. Long-lived complexes and signatures of chaos in ultracold K₂+Rb collisions. *Phys. Rev. A* **2017**, *96*, 062707.
- (31) Ospelkaus, S.; Ni, K.-K.; Wang, D.; de Miranda, M. H. G.; Neyenhuis, B.; Quéméner, G.; Julienne, P. S.; Bohn, J. L.; Jin, D. S.; Ye, J. Quantum-state controlled chemical reactions of ultracold KRb molecules. *Science* **2010**, *327*, 853–857.
- (32) A notable exception is vibrational excitation of the reactant molecule, for which abstraction reactions can also become barrierless and exhibit a potential well (e.g., H(D) + H₂($v \geq 5$)) (See Refs. [25](#), [27](#), [28](#)).
- (33) Quéméner, G.; Bohn, J. L. Strong dependence of ultracold chemical rates on electric dipole moments. *Phys. Rev. A* **2010**, *81*, 022702.
- (34) Kotochigova, S. Dispersion interactions and reactive collisions of ultracold polar molecules. *New J. Phys.* **2010**, *12*, 073041.
- (35) Idziaszek, Z.; Julienne, P. S. Universal rate constants for reactive collisions of ultracold molecules. *Phys. Rev. Lett.* **2010**, *104*, 113202.
- (36) Tscherbul, T. V.; Kłos, J. Magnetic tuning of ultracold barrierless chemical reactions. *Phys. Rev. Research* **2020**, *2*, 013117.
- (37) Makrides, C.; Hazra, J.; Pradhan, G. B.; Petrov, A.; Kendrick, B. K.; González-Lezana, T.; Balakrishnan, N.; Kotochigova, S. Ultracold chemistry with alkali-metal–rare-earth molecules. *Phys. Rev. A* **2015**, *91*, 012708.
- (38) Li, H.; Li, M.; Makrides, C.; Petrov, A.; Kotochigova, S. Universal scattering of ultracold atoms and molecules in optical potentials. *Atoms* **2019**, *7*, 36.

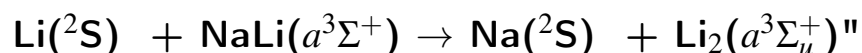
- (39) Kendrick, B. K.; Li, H.; Li, M.; Kotochigova, S.; Croft, J. F. E.; Balakrishnan, N. Non-adiabatic quantum interference in the ultracold $\text{Li} + \text{LiNa} \rightarrow \text{Li}_2 + \text{Na}$ reaction. *Phys. Chem. Chem. Phys.* **2021**, *23*, 5096–5112.
- (40) Kendrick, B. K. Quantum reactive scattering calculations for the cold and ultracold $\text{Li} + \text{LiNa} \rightarrow \text{Li}_2 + \text{Na}$ reaction. *J. Chem. Phys.* **2021**, *154*, 124303.
- (41) Julienne, P. S.; Hanna, T. M.; Idziaszek, Z. Universal ultracold collision rates for polar molecules of two alkali-metal atoms. *Phys. Chem. Chem. Phys.* **2011**, *13*, 19114–19124.
- (42) Frye, M. D.; Julienne, P. S.; Hutson, J. M. Cold atomic and molecular collisions: Approaching the universal loss regime. *New J. Phys.* **2015**, *17*, 045019.
- (43) Krems, R. V. Cold Controlled Chemistry. *Phys. Chem. Chem. Phys.* **2008**, *10*, 4079–4092.
- (44) Wang, T. T.; Heo, M.-S.; Rvachov, T. M.; Cotta, D. A.; Ketterle, W. Deviation from universality in collisions of ultracold $^6\text{Li}_2$ molecules. *Phys. Rev. Lett.* **2013**, *110*, 173203.
- (45) Yang, H.; Zhang, D.-C.; Liu, L.; Liu, Y.-X.; Nan, J.; Zhao, B.; Pan, J.-W. Observation of magnetically tunable Feshbach resonances in ultracold $^{23}\text{Na}^{40}\text{K} + ^{40}\text{K}$ collisions. *Science* **2019**, *363*, 261.
- (46) Park, J. J.; Lu, Y.-K.; Jamison, A. O.; Tscherbul, T. V.; Ketterle, W. A Feshbach resonance in collisions between triplet ground-state molecules. *Nature* **2023**, *614*, 54–58.
- (47) Rvachov, T. M.; Son, H.; Sommer, A. T.; Ebadi, S.; Park, J. J.; Zwierlein, M. W.; Ketterle, W.; Jamison, A. O. Long-lived ultracold molecules with electric and magnetic dipole moments. *Phys. Rev. Lett.* **2017**, *119*, 143001.
- (48) Son, H.; Park, J. J.; Ketterle, W.; Jamison, A. O. Collisional cooling of ultracold molecules. *Nature* **2020**, *580*, 197–200.
- (49) Cvitaš, M. T.; Soldán, P.; Hutson, J. M.; Honvault, P.; Launay, J.-M. Ultracold $\text{Li} + \text{Li}_2$ collisions: Bosonic and fermionic cases. *Phys. Rev. Lett.* **2005**, *94*, 033201.

- (50) Cvitaš, M. T.; Soldán, P.; Hutson, J. M.; Honvault, P.; Launay, J.-M. Interactions and dynamics in Li + Li₂ ultracold collisions. *J. Chem. Phys.* **2007**, *127*, 074302.
- (51) Soldán, P.; Cvitaš, M. T.; Hutson, J. M.; Honvault, P.; Launay, J.-M. Quantum dynamics of ultracold Na + Na₂ collisions. *Phys. Rev. Lett.* **2002**, *89*, 153201.
- (52) Quéméner, G.; Honvault, P.; Launay, J.-M.; Soldán, P.; Potter, D. E.; Hutson, J. M. Ultracold quantum dynamics: Spin-polarized K + K₂ collisions with three identical bosons or fermions. *Phys. Rev. A* **2005**, *71*, 032722.
- (53) Cvitaš, M. T.; Soldán, P.; Hutson, J. M.; Honvault, P.; Launay, J.-M. Ultracold collisions involving heteronuclear alkali metal dimers. *Phys. Rev. Lett.* **2005**, *94*, 200402.
- (54) Hutson, J. M.; Soldán, P. Molecular collisions in ultracold atomic gases. *Int. Rev. Phys. Chem.* **2007**, *26*, 1–28.
- (55) Moore, J. H. Investigation of the Wigner spin rule in collisions of N⁺ with He, Ne, Ar, N₂, and O₂. *Phys. Rev. A* **1973**, *8*, 2359–2362.
- (56) Tscherbil, T. V.; Krems, R. V. Controlling electronic spin relaxation of cold molecules with electric fields. *Phys. Rev. Lett.* **2006**, *97*, 083201.
- (57) Haze, S.; D’Incao, J. P.; Dorer, D.; Deiß, M.; Tiemann, E.; Julienne, P. S.; Denschlag, J. H. Spin-conservation propensity rule for three-body recombination of ultracold Rb atoms. *Phys. Rev. Lett.* **2022**, *128*, 133401.
- (58) Abrahamsson, E.; Tscherbil, T. V.; Krems, R. V. Inelastic collisions of cold polar molecules in nonparallel electric and magnetic fields. *J. Chem. Phys.* **2007**, *127*, 044302.
- (59) Knowles, P. J.; Werner, H.-J. An efficient method for the evaluation of coupling coefficients in configuration interaction calculations. *Chem. Phys. Lett.* **1988**, *145*, 514–522.
- (60) Werner, H.-J.; Knowles, P. J. An efficient internally contracted multiconfiguration–reference configuration interaction method. *J. Chem. Phys.* **1988**, *89*, 5803–5814.

- (61) Knowles, P. J.; Werner, H.-J. An efficient second-order MC SCF method for long configuration expansions. *Chem. Phys. Lett.* **1985**, *115*, 259–267.
- (62) Werner, H.-J.; Knowles, P. J. A second order multiconfiguration SCF procedure with optimum convergence. *J. Chem. Phys.* **1985**, *82*, 5053–5063.
- (63) Werner, H.-J.; *et al.*, MOLPRO, version 2015.1, a package of *ab initio* programs. 2015.
- (64) See Supporting Information at [URL] for details of our *ab initio* and quantum reactive scattering calculations, including convergence tests, and for state-to-state reaction rates influenced by the potential scaling.
- (65) Lesiuk, M.; Musiał, M.; Moszynski, R. Potential-energy curve for the $a^3\Sigma_u^+$ state of a lithium dimer with Slater-type orbitals. *Phys. Rev. A* **2020**, *102*, 062806.
- (66) Parker, G. A.; Walker, R. B.; Kendrick, B. K.; T Pack, R. Accurate quantum calculations on three-body collisions in recombination and collision-induced dissociation. I. Converged probabilities for the H+Ne₂ system. *J. Chem. Phys.* **2002**, *117*, 6083–6102.
- (67) Gronowski, M.; Koza, A. M.; Tomza, M. Ab initio properties of the NaLi molecule in the $a^3\Sigma^+$ electronic state. *Phys. Rev. A* **2020**, *102*, 020801.
- (68) D’Incao, J. P. Few-body physics in resonantly interacting ultracold quantum gases. *J. Phys. B* **2018**, *51*, 043001.
- (69) Colavecchia, F. D.; Burke, J. P.; Stevens, W. J.; Salazar, M. R.; Parker, G. A.; T Pack, R. The potential energy surface for spin-aligned Li₃ and the potential energy curve for spin-aligned Li₂. *J. Chem. Phys.* **2003**, *118*, 5484–5495.
- (70) Gribakin, G. F.; Flambaum, V. V. Calculation of the scattering length in atomic collisions using the semiclassical approximation. *Phys. Rev. A* **1993**, *48*, 546–553.
- (71) Frye, M. D.; Hutson, J. M. Complexes formed in collisions between ultracold alkali-metal diatomic molecules and atoms. *New J. Phys.* **2021**, *23*, 125008.

- (72) Morita, M.; Krems, R. V.; Tscherebul, T. V. Universal probability distributions of scattering observables in ultracold molecular collisions. *Phys. Rev. Lett.* **2019**, *123*, 013401.
- (73) Croft, J. F. E.; Hazra, J.; Balakrishnan, N.; Kendrick, B. K. Symmetry and the geometric phase in ultracold hydrogen-exchange reactions. *J. Chem. Phys.* **2017**, *147*, 074302.
- (74) Lara, M.; Bohn, J. L.; Potter, D.; Soldán, P.; Hutson, J. M. Ultracold Rb-OH collisions and prospects for sympathetic cooling. *Phys. Rev. Lett.* **2006**, *97*, 183201.
- (75) Tscherebul, T. V.; Kłos, J.; Buchachenko, A. A. Ultracold spin-polarized mixtures of $^2\Sigma$ molecules with S -state atoms: Collisional stability and implications for sympathetic cooling. *Phys. Rev. A* **2011**, *84*, 040701.
- (76) Morita, M.; Kłos, J.; Buchachenko, A. A.; Tscherebul, T. V. Cold collisions of heavy $^2\Sigma$ molecules with alkali-metal atoms in a magnetic field: Ab initio analysis and prospects for sympathetic cooling of SrOH($^2\Sigma^+$) by Li(2S). *Phys. Rev. A* **2017**, *95*, 063421.
- (77) Morita, M.; Kosicki, M. B.; Żuchowski, P. S.; Tscherebul, T. V. Atom-molecule collisions, spin relaxation, and sympathetic cooling in an ultracold spin-polarized Rb(2S) – SrF($^2\Sigma^+$) mixture. *Phys. Rev. A* **2018**, *98*, 042702.

Supporting Information for
"Signatures of Non-universal Quantum Dynamics
of Ultracold Chemical Reactions
of Polar Alkali-dimer Molecules with Alkali-metal Atoms:



Masato Morita¹, Brian K. Kendrick² Jacek Kłos^{3,4},
 Svetlana Kotochigova⁴, Paul Brumer^{1*} and Timur V. Tscherbul^{5*}

¹*Chemical Physics Theory Group, Department of Chemistry, and Center for Quantum Information and Quantum Control, University of Toronto, Toronto, Ontario, M5S 3H6, Canada*

²*Theoretical Division (T-1, MS B221), Los Alamos National Laboratory, Los Alamos, New Mexico 87545, USA,*

³*Joint Quantum Institute, University of Maryland, College Park, Maryland, 20742, USA*

⁴*Department of Physics, Temple University, Philadelphia, PA 19122, USA*

⁵*Department of Physics, University of Nevada, Reno, NV, 89557, USA*

E-mail: paul.brumer@utoronto.ca, ttscherbul@unr.edu

In this Supporting Information (SI), we present the details of *ab initio* calculations for the potential energy surface (PES) of the NaLi₂ (1⁴A') reaction complex (Section S-I). Sections S-II and S-III provide the methodological and computational details of our quantum reactive scattering calculations using the APH3D code. Section S-III discusses convergence tests. Section S-IV describes the universal loss (total reaction) rate, along with the values of parameters for the Li+NaLi(*a*³Σ⁺) system. The λ dependence of the reaction rate (including the effects of exchange symmetry of the Li nuclei) is discussed in detail in Section S-V, which also contains the state-to-state reaction rates. The reactive and elastic cross sections and elastic-to-inelastic ratios calculated with the pairwise PES (λ = 0) are presented in Section S-VI.

S-I Potential energy surface

The spin conserving reaction $\text{Li}(^2\text{S}) + \text{NaLi}(a^3\Sigma^+, v=0, j=0) \rightarrow \text{Li}_2(a^3\Sigma_u^+, v', j') + \text{Na}(^2\text{S})$ proceeds on the $1^4A'$ PES. The calculations of the PES, $V_{1^4A'}(r_a, r_b, \alpha)$, have been performed on a set of discrete grids of NaLi_2 geometries described by two NaLi bond lengths r_a and r_b and the bond angle α for $\text{Li}(a)\text{-Na-Li}(b)$. The grid consists of bond lengths r_a and r_b from $3.75a_0$ to $14a_0$ with a step of $0.25a_0$ (where a_0 is the Bohr radius), and the bond angle α from 0° to 180° with a step of 5° with additional α values of $1^\circ, 2^\circ, 4^\circ, 8^\circ$ and 179° for near collinear geometries. We performed the electronic structure calculations using MOLPRO.^{S1}

In our reactive scattering calculations the PES is represented as the sum of pairwise (two-body) and three-body interactions

$$V_{1^4A'}(r_{\text{Li-Li}'}, r_{\text{Na-Li}}, r_{\text{Na-Li}'}) = V_{1^4A'}^{\text{pairwise}}(r_{\text{Li-Li}'}, r_{\text{Na-Li}}, r_{\text{Na-Li}'}) + \lambda V_{1^4A'}^{\text{3-body}}(r_{\text{Li-Li}'}, r_{\text{Na-Li}}, r_{\text{Na-Li}'}), \quad (\text{S1})$$

where arguments specifying the geometry of NaLi_2 are transformed into the three bond lengths to match the interface of the APH3D code (see Section S-II), $r_{\text{A-B}}$ denotes the bond distance between A and B, the prime for Li' is introduced to make a distinction of two identical Li nuclei. The pairwise (two-body) interaction $V_{1^4A'}^{\text{pairwise}}$ is decomposed into the sum of diatomic interaction potentials as

$$V_{1^4A'}^{\text{pairwise}}(r_{\text{Li-Li}'}, r_{\text{Na-Li}}, r_{\text{Na-Li}'}) = V_{a^3\Sigma_u^+}^{\text{Li}_2}(r_{\text{Li-Li}'}) + V_{a^3\Sigma^+}^{\text{NaLi}}(r_{\text{Na-Li}}) + V_{a^3\Sigma^+}^{\text{NaLi}}(r_{\text{Na-Li}'}), \quad (\text{S2})$$

where $V^{\text{A-B}}$ in the right-hand-side of the equation denotes the potential energy curve for the diatomic AB molecule. This additive pairwise potential $V_{1^4A'}^{\text{pairwise}}$ dominates the long-range behaviour of the total potential of $V_{1^4A'}$. For $V_{a^3\Sigma^+}^{\text{NaLi}}$ and $V_{a^3\Sigma_u^+}^{\text{Li}_2}$ in Eq. (S2), we employ the accurate *ab initio* potential energy curves.^{S2,S3} The non-additive three-body interaction, $V_{1^4A'}^{\text{3-body}}$, governs the short-range dynamics. We use accurate electronic structure calculations to obtain the three-body interaction. The calculations and the fitting procedure are described below. Because V^{pairwise} and $V^{\text{3-body}}$ are smooth functions of the internal coordinates, so is the total potential V given in Eq. (S1) at any λ .

The details of the present electronic structure calculations are the same as previously published for the spin doublet NaLi_2 potentials.^{S4} During the calculations of the global $1^4A'$ potential we encountered a conical intersection and an avoided crossing between the $1^4A'$ and $2^4A'$ states located on the repulsive wall of the PES, but still at relatively low energies to affect the fit. The appearance of the conical intersection causes difficulties in the fitting procedure of the three-body term by expansion in Legendre polynomials and interpolation of the 2-dimensional radial coefficients as functions of bond distances. Because we fit the lowest $1^4A'$ adiabatic PES instead of the diabatic one, we need a procedure to smooth out numerical instabilities caused by abrupt changes of the potential in the vicinity of the conical intersection seam that project also to long distances. To smooth out the kinks in the RKHS fits of the three-body Legendre expansion^{S4} we resorted to smoothly connecting the analytical Axilrod-Teller three-body dispersion term^{S5,S6} to the short-

range three-body fit. In order to accomplish this, we need the C_9 long-range dispersion coefficient for the NaLi_2 ($1^4A'$) trimer.

We calculated the C_9 long-range dipole dispersion coefficient of the $V_{1^4A'}^{3\text{-body}}$ potential using imaginary frequency-dependent dipole polarizabilities of Li and Na atoms of Derevianko *et al.*^{S7} using the following formula:

$$C_9 = \frac{3}{\pi} \int \alpha_{\text{Li}}(i\omega) \alpha_{\text{Li}}(i\omega) \alpha_{\text{Na}}(i\omega) d\omega. \quad (\text{S3})$$

We used 50 Gauss-Legendre quadrature nodes for the numerical evaluation of the above integral and we obtained the value of $C_9 = 175597.73 E_h a_0^9$, which is close to the literature value of Peña *et al.*^{S5} of $17.566 \times 10^4 E_h a_0^9$. This procedure has a minimal effect on the global minimum region of the full $1^4A'$ potential.

To obtain an analytical representation of $V_{1^4A'}(r_a, r_b, \alpha)$ from the *ab initio* grid points, we apply a fit or interpolation procedure similar to that described in Ref.^{S4} Namely, we first obtain the non-additive three-body contribution by subtracting the pairwise (two-body) potential constructed from the diatomic $\text{NaLi}(a^3\Sigma^+)$ and $\text{Li}_2(a^3\Sigma_u^+)$ potentials also obtained by MOLPRO calculations. This non-additive three-body contribution is then expanded in a series of Legendre polynomials $P_l(\cos \alpha)$ with l up to $l_{\text{max}} = 8$, where the two-dimensional $v_l(r_a, r_b)$ radial expansion coefficients are interpolated. The short-range three-body contribution is smoothly connected using a switching function to the long-range Axilrod-Teller dispersion potential $V_{3b}^{\text{lr}} = C_9(1 + \cos \alpha_1 \cos \alpha_2 \cos \alpha_3)/(r_1^3 r_2^3 r_3^3)$, where r_i and α_i are the lengths of the sides and inner angles of the triangle formed by the three atoms and the van der Waals three-body dispersion coefficient C_9 is computed from the imaginary-frequency dependent polarizabilities^{S7} of the Na and Li atoms as described above. Here, E_h is the Hartree energy. The switching function is the sigmoid function $sw(r_i) = (1 - \tanh[\beta_{\text{sw}}(r_i - r_{\text{sw}})])/2$ for $i = 1, 2$, or 3 where $r_{\text{sw}} = 10.0 a_0$ and $\beta_{\text{sw}} = 1.0/a_0$ for all i .

S-II Quantum reactive scattering calculations

The quantum mechanical dynamics of the $\text{Li}(^2S) + \text{NaLi}(a^3\Sigma^+, v = 0, j = 0) \rightarrow \text{Li}_2(a^3\Sigma_u^+, v', j') + \text{Na}(^2S)$ reaction on the $1^4A'$ PES is explored by performing the rigorous approach based on the adiabatically adjusting principal axes hyperspherical (APH) coordinates method.^{S8,S9} We only briefly summarize the method and calculation procedures since several publications describe the detailed information about the APH coordinate method and its implementation (APH3D program suite).^{S4,S10,S11} The values of parameters used in the present scattering calculations are described in Section S-III.

The time-independent Schrödinger equation for the triatomic system is written in the hyperspherical coordinates as

$$\left[-\frac{\hbar^2}{2\mu\rho^5} \frac{\partial}{\partial\rho} \rho^5 \frac{\partial}{\partial\rho} + \frac{\hat{\Lambda}^2}{2\mu\rho^2} + V(\rho, \tilde{\theta}, \phi) \right] \Psi(\rho, \tilde{\theta}, \phi, \alpha, \beta, \gamma) = E\Psi(\rho, \tilde{\theta}, \phi, \alpha, \beta, \gamma), \quad (\text{S4})$$

where μ is the three-body reduced mass defined by using the mass of each atom as $\sqrt{m_A m_B m_C / (m_A + m_B + m_C)}$, $\hat{\Lambda}$ is the grand angular momentum operator, V denotes the PES, E denotes the total energy, ρ is the hyperradius that is the radial coordinate corresponding to a symmetric stretch motion of the triatomic complex, $\tilde{\theta}$ is the polar angle corresponding to a bending motion and related to the θ of Pack and Parker as $\tilde{\theta} = \pi - 2\theta$, ϕ is the azimuthal angle corresponding to an internal pseudo-rotational motion and related to the χ of Pack and Parker as $\phi = 2\chi$, the three Euler angles α, β, γ specify the orientation of the body-fixed (BF) frame relative to the space-fixed (SF) frame. The z-axis of the BF frame directs perpendicular to the plane of triatomic complex and the x and y axes are chosen to lie along the instantaneous principal axes of inertia. For a given total angular momentum J , inversion parity p and exchange symmetry q for the identical atoms, the wave function Ψ is expanded using the 5D surface functions Φ that are the functions of hyperangles $\tilde{\theta}$ and ϕ , and three Euler angles as

$$\Psi^{JMpq}(\rho, \tilde{\theta}, \phi, \alpha, \beta, \gamma) = 4\sqrt{2} \sum_n^{N_{\text{ch}}} \rho^{-5/2} \zeta_n^{Jpq}(\rho) \Phi_n^{JMpq}(\tilde{\theta}, \phi, \alpha, \beta, \gamma; \rho_\xi), \quad (\text{S5})$$

where the N_{ch} specifies the number of coupled channels, and ζ are the ρ -dependent expansion coefficients. The surface functions are obtained by solving the following eigenproblem at each ρ_ξ ,

$$\left[\frac{\tilde{\Lambda}^2}{2\mu\rho_\xi^2} + \frac{15\hbar^2}{8\mu\rho_\xi^2} + V(\rho_\xi, \tilde{\theta}, \phi) \right] \Phi_n^{JMpq}(\tilde{\theta}, \phi, \alpha, \beta, \gamma; \rho_\xi) = \varepsilon_n^{Jpq}(\rho_\xi) \Phi_n^{JMpq}(\tilde{\theta}, \phi, \alpha, \beta, \gamma; \rho_\xi). \quad (\text{S6})$$

Outside the strongly interacting short-range region, where the inter-arrangement coupling is negligible, we use the Delves hyperspherical coordinates. In contrast to Eq. (S5), the total wave function is expanded in a set of the products of ρ -dependent vibrational wavefunctions and the angular functions in each arrangement channel of τ as

$$\Psi^{JMpq}(\rho, \theta, \hat{S}_\tau, \hat{s}_\tau) = 2 \sum_n^{N_{\text{ch}}} \rho^{-5/2} \zeta_n^{Jpq}(\rho) \frac{\Upsilon_n^{Jq}(\theta_\tau; \rho)}{\sin 2\theta_\tau} \mathcal{Y}_n^{JMpq}(\hat{S}_\tau, \hat{s}_\tau), \quad (\text{S7})$$

where Υ denotes vibrational wavefunction, \mathcal{Y} denotes coupled-angular momentum with the mass-scaled Jacobi vectors \hat{S}_τ and \hat{s}_τ in the arrangement channel of τ . Although the hyperradius ρ is the same as in the APH coordinates, the hyperangles are different and depend on τ and are defined as $\theta_\tau = \tan^{-1}(s_\tau/S_\tau)$ and $\Theta_\tau = \cos^{-1}(\hat{S}_\tau \cdot \hat{s}_\tau / S_\tau s_\tau)$. We note that the above equation is in the SF coordinate representation. The 1D equation for the vibration is given as

$$\left\{ -\frac{\hbar^2}{2\mu\rho_\xi^2} \left[\frac{\partial^2}{\partial \theta_\tau^2} - \frac{j_\tau(j_\tau + 1)}{\sin^2 \theta_\tau} - \frac{l_\tau(l_\tau + 1)}{\cos^2 \theta_\tau} \right] + V_\tau(\rho_\xi \sin \theta_\tau) \right\} \Upsilon_n(\theta_\tau; \rho_\xi) = \mathcal{E}_n(\rho_\xi) \Upsilon_n(\theta_\tau; \rho_\xi), \quad (\text{S8})$$

where j_τ is rotational quantum number of the diatomic molecule, l_τ is the orbital angular momentum of the atom around the center of mass for the diatomic molecule, V_τ is the two-body potential for the molecule in the arrangement τ . The equation parametrically depends on the values of j_τ and l_τ , thus the index n is specified with collective quantum numbers of $\{v_\tau, j_\tau, l_\tau\}$, where v_τ is the quantum number for the vibration.

In both the APH and Delves coordinates, the coupled-channel equations to be satisfied by the expansion coefficients of $\zeta(\rho)$ are obtained by substituting the Eqs. (S5) and (S7) into the total wave function Ψ in the Schrödinger equation. The Hamiltonian in the Delves coordinates is similar to that in the APH coordinates Eq. (S4) but the expression for $\hat{\Lambda}^2$ is different.^{S12} The obtained coupled-channel equations are solved based on the log-derivative propagation method followed by the matching procedure to the scattering boundary condition at a large asymptotic ρ value to obtain the S-matrix.^{S8,S12}

S-III Computational details

All quantum mechanical scattering calculations in this study are performed with the APH3D program suite developed at the Los Alamos National Laboratory. Here, we summarize the relevant parameters employed in our calculations. The masses for ^{23}Na and ^6Li are 22.9897692808 amu and 6.0151227945 amu, respectively. At short range ($6 \leq \rho \leq 40a_0$) the time independent Schrödinger equation is described in the APH coordinates, and the range is divided into $0.1 a_0$ wide sectors. The surface functions to expand the total wave function within a sector are obtained by solving the eigenproblem at the center of each sector as described below. The log-derivative propagation is carried out using the diabatic-by-sector method with 200 propagation steps per each sector.

To construct the Hamiltonian matrix for the eigenproblem, the hyperangles are expanded with a primitive basis of Jacobi polynomials in $\tilde{\theta}$ and complex exponential functions in ϕ whose sizes are specified by $l_{\text{max}} = 159$ and $m_{\text{max}} = 320$.^{S9} The actual numbers of basis functions are given by $l_{\text{max}} + 1$ and $2m_{\text{max}} + 1$, respectively, and a the discrete variable representation (DVR) is used in $\tilde{\theta}$ rather than the finite basis representation. While the original dimension of the Hamiltonian matrix is 102560 for $J = 0^+$ (even), actual dimension of the matrix is typically reduced to 40000-

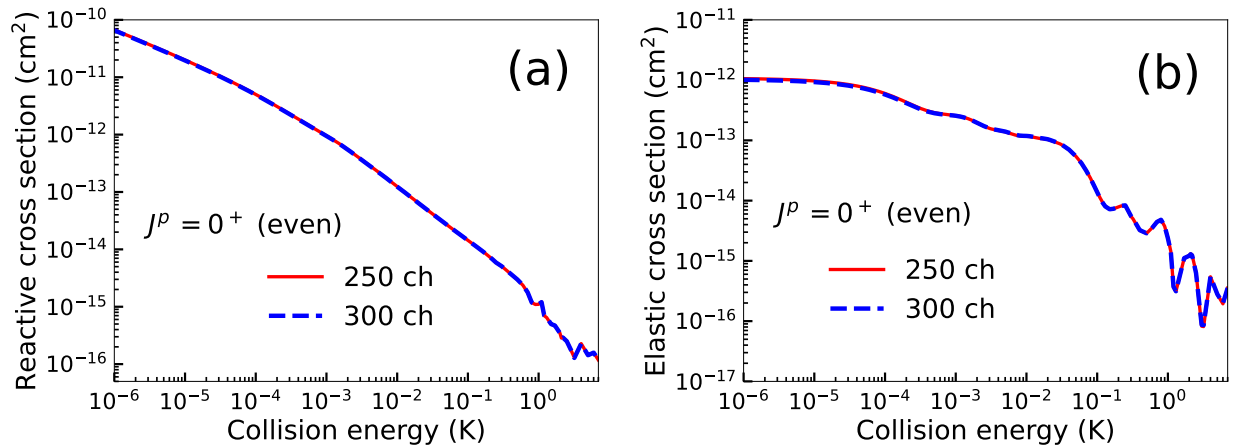


Figure S1: Reactive (a) and elastic (b) cross sections as a function of collision energy calculated using coupled-channel basis sets containing 250 and 300 channels for $J = 0^+$ and even exchange symmetry. The statistical factor of $1/3$ is not applied.

60000 by employing the Sequential Diagonalization Truncation (SDT) method. The number of channels used in the coupled-channel calculation is 250 with $J = 0$ for each inversion and exchange symmetry. We increase the number of channels to 300 for $J = 1$.

Figure S1 shows the convergence of the reactive and elastic cross sections as a function of collision energy with 250 channels for $J = 0^+$ with even exchange symmetry. Beyond $\rho = 40a_0$, there is no interaction between the different reaction arrangements (see main text), and the coupled channel equations are solved in the Delves coordinates as described above. The three-body term decays rapidly with increasing ρ and becomes negligible at $\rho \geq 22a_0$. Thus, the PES and the associated adiabatic potentials do not depend on λ at $\rho \geq 22a_0$. The number of channels, propagation sectors, and log-derivative propagation steps within each sector used in the Delves propagation are the same as those used in the APH region.

After reaching the end of the propagation grid at $\rho_{\max} = 400a_0$, the reactance (K) matrix is calculated in the asymptotic Jacobi basis, and the full state-to-state S-matrix is obtained from the K-matrix as described in Ref.^{S12} Figure S2 shows the ρ_{\max} dependence of the calculated reactive and elastic cross sections. Despite the relatively slow ρ_{\max} convergence in the low energy region observed in Fig. S2(a), we can still obtain an accurate reactive cross section with $\rho_{\max} = 400a_0$. On the other hand, the elastic cross section exhibits extremely slow convergence with respect to ρ_{\max} , especially in the collision energy range between 10^{-5} to 10^{-4} K.

The elastic cross section is typically more difficult to converge, however, the very large $\rho_{\max} > 1000a_0$ is counterintuitive. Small oscillations in the elastic cross sections are seen in the black, red, blue and green curves near 2 mK, 0.4 mK, 0.1 mK and 0.02 mK, respectively. These oscillations are most likely due to the tiny difference between the Delves energies computed at ρ_{\max} and the asymptotic Jacobi energies. This energy step discontinuity is due to the difference between the two coordinate systems, for large ρ the one-dimensional diatomic potential energy curve for each arrangement channel in Delves coordinates is slightly different than the asymptotic Jacobi one. As ρ_{\max} is increased the energy step decreases, which is consistent with the observed oscillations

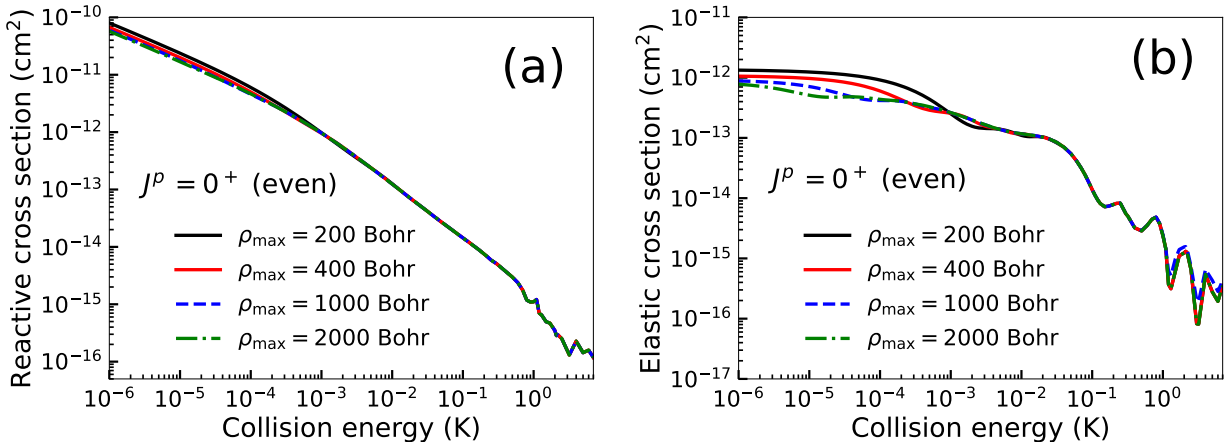


Figure S2: Reactive (a) and elastic (b) cross sections as a function of collision energy for different maximum hyper radius (ρ_{\max}) in the log-derivative propagation for solving the coupled-channel equation for $J = 0^+$ and the even exchange symmetry. Statistical factor of 1/3 is not multiplied.

moving to lower collision energies as ρ_{\max} is increased. The energy step is always present and can lead to unphysical self-interference effects that appear to be more significant for this system.

We conclude that it is necessary to use a vary large ρ_{\max} to achieve complete numerical convergence of the elastic cross section for ultracold vdW reactions. These considerations only apply to the elastic cross sections. As such, they do not affect the discussions and conclusions described in this main text because our primary interest is in the reaction processes and order-of-magnitude estimates of the elastic-to-inelastic ratio.

S-IV Universal rate

$$K_{l=0}^{\text{UM}} = \frac{4\pi\hbar}{\mu} \bar{a} \quad (\text{S9})$$

$$\bar{a} = \frac{2\pi}{\Gamma(1/4)^2} \left(\frac{2\mu C_6}{\hbar^2} \right)^{\frac{1}{4}} \quad (\text{S10})$$

Here, we describe the universal rate for the s -wave ($l = 0$) K_0^{UM} and p -wave ($l = 1$) $K_1^{\text{UM}}(E)$ based on the universal model (UM).^{S13,S14} The energy independent s -wave universal rate is

$$K_0^{\text{UM}} = \frac{4\pi\hbar}{\mu} \bar{a}, \quad (\text{S11})$$

where μ is the reduced mass for the ${}^6\text{Li}+{}^{23}\text{Na}{}^6\text{Li}$ system, the mean scattering length \bar{a} is given as^{S15}

$$\bar{a} = \frac{4\pi R_6}{\Gamma(1/4)^2} = \frac{2\pi}{\Gamma(1/4)^2} \left(\frac{2\mu C_6}{\hbar^2} \right)^{\frac{1}{4}}, \quad (\text{S12})$$

where $R_6 = (2\mu C_6/\hbar^2)^{\frac{1}{4}}/2$ is a characteristic length. As stated in the main text, we use the *ab initio* value $C_6 = 2891.15 E_h/a_0^6$ for the long-rang dispersion coefficient between Li and NaLi. The universal reaction rate is $K_0^{\text{UM}} = 3.45 \times 10^{-10} \text{ cm}^3/\text{s}$ in the s -wave regime. The p -wave contribution to the universal rate is^{S13,S14}

$$K_1^{\text{UM}}(E) = \frac{12\pi\hbar}{\mu} (k\bar{a})^2 \bar{a}_1, \quad (\text{S13})$$

where $\bar{a}_1 = \bar{a}\Gamma(1/4)^6/(144\pi^2\Gamma(3/4)^2)$. The p -wave contribution is negligible compared to K_0 as $E \rightarrow 0$ ($k \rightarrow 0$). Note that the universal rate does not depend on the short-range behavior of the PES.

S-V λ -scaling

In the main text, the total rate for the chemical reaction $\text{Li} + \text{NaLi}(v = 0, j = 0) \rightarrow \text{Li}_2 + \text{Na}$ is obtained by adding together the even and odd contributions due to the exchange symmetry of

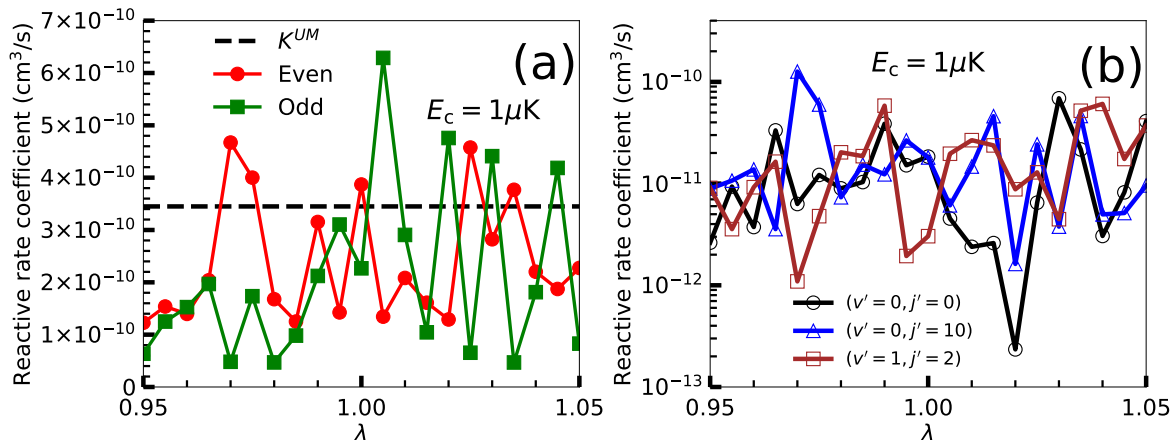


Figure S3: (a) Total reaction rate as a function of the scaling parameter λ at $E_c = 10^{-6}\text{K}$ ($1\mu\text{K}$) for even and odd exchange symmetries of identical Li nuclei. The statistical factors of $1/3$ and $2/3$ for even and odd symmetries are not applied. The dashed line indicates the universal rate, $K^{UM} = 3.45 \times 10^{-10} \text{ cm}^3/\text{s}$. (b) State-to-state reaction rates to the final states $(v' = 0, j' = 0)$, $(v' = 0, j' = 10)$, and $(v' = 1, j' = 2)$ as a function λ at $E_c = 10^{-6}\text{K}$ for the even exchange symmetry and $J = 0^+$.

identical Li nuclei. This addition leads to an averaging effect. Indeed, in Fig. S3(a) we see a higher contrast in the reaction rate for each individual exchange symmetry plotted as a function of λ . We note that each exchange symmetry contribution is a sum of state-to-state contributions, and hence already contains a substantial amount of averaging as stated in the main text.

In panel Fig. S3(b), we show the behavior of the state-to-state reaction rates as functions of λ for several product states (v', j') of even exchange symmetry and $J = 0^+$. We observe a very pronounced λ -dependence of the state-to-state rates, which can vary by several orders of magnitude over a narrow interval of λ ($\pm 1\%$). This shows that state-to-state collision dynamics are profoundly affected by the detailed short-range behavior of the PES.

In Fig. S4, we show the elastic rates (upper panel) and all possible state-to-state reaction rates (lower panels) as a functions of λ . The elastic rate varies by several orders of magnitude as a function of λ for each exchange symmetry. While the variations of the elastic and state-to-state reaction rates might have a common origin (such as near-threshold resonances), a more detailed study using finer λ grids is required to establish the existence of a correlation between the elastic and state-to-state reaction rates. The total reaction rates for both exchange symmetries vary strongly with λ due to the incomplete averaging of the state-to-state rates.

S-VI Results with pairwise PES

To explore the effect of three-body interactions on ultracold reaction observables, we performed reactive scattering computations on the two-body pairwise PES given by Eq. (S2). Note that the

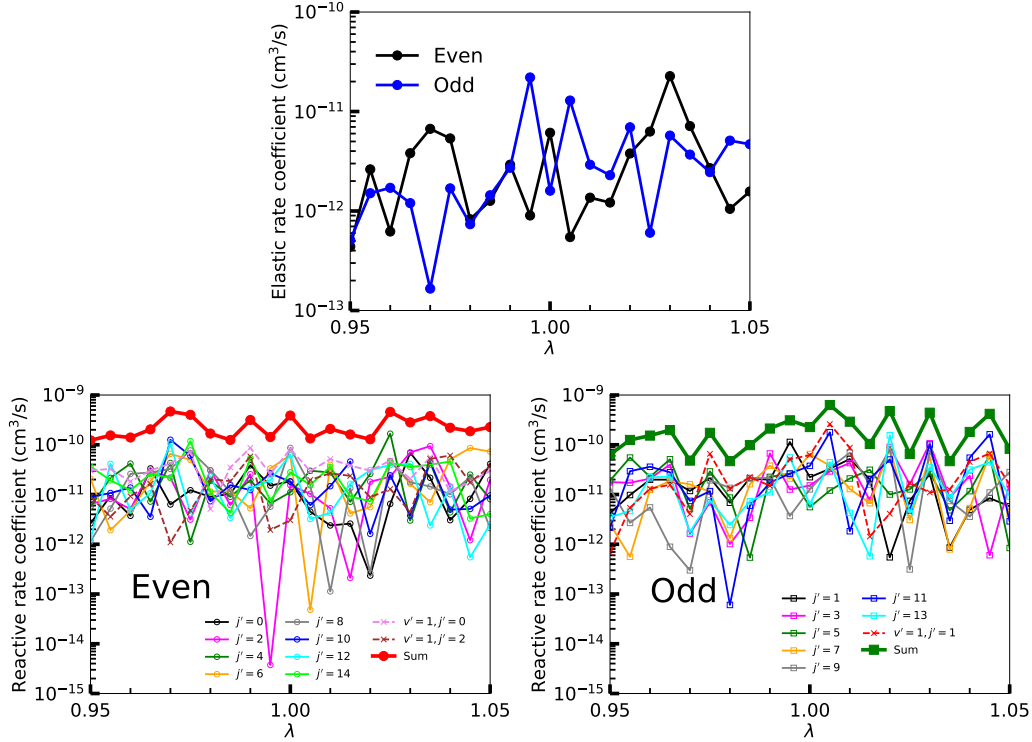


Figure S4: Upper panel: The λ dependence of the elastic rate for $\text{Li}+\text{NaLi}(v=0, j=0)$ collisions at $E_c = 1 \mu\text{K}$. Lower panels show state-to-state reaction rates to all energetically accessible final states ($v' = 0, j' = 0 - 14$ and $v' = 1, j' = 0 - 2$) as a function of λ at $E_c = 1 \mu\text{K}$ for even (left) and odd (right) exchange symmetries. The vibrational quantum number $v' = 0$ is omitted in the legends. The statistical factors of $1/3$ and $2/3$ are not applied.

pairwise PES has the same long-range behavior as the full PES given by Eq. (S1). Thus, the only difference between these two PESs comes from three-body interactions at short range, as shown in Fig. S6.

Figure S5 shows the reactive and elastic cross sections and their ratio calculated using the pairwise PES (Eq. (S2)). We observe that the contribution of the odd exchange symmetry for the identical Li nuclei (green) is almost 10 times larger than that of the even exchange symmetry in the s -wave regime for the reactive cross sections. On the other hand, we see comparable contributions from both exchange symmetries in the full PES results with $\lambda = 1$ (see the main text). This implies that short-range three-body interactions can have a significant effect on the dependence of reactive scattering cross sections on the exchange symmetry. The large difference between the exchange symmetries is most likely due to quantum interference between the Li exchange and non-exchange processes as observed for $\text{H} + \text{HD} \rightarrow \text{H} + \text{HD}$,^{S17} although it is difficult to determine the extent of the interference based on the shape of the PES.

Figure S5(c) shows that the reactive cross section is much larger than the elastic cross section at ultralow energies. The total reaction rate ($2.78 \times 10^{-10} \text{ cm}^3/\text{s}$) calculated on the pairwise PES agrees well with the universal rate ($3.45 \times 10^{-10} \text{ cm}^3/\text{s}$) at $E = 1 \mu\text{K}$ as shown in Fig. S5 (d) and is comparable with the rate ($2.83 \times 10^{-10} \text{ cm}^3/\text{s}$) calculated with the full PES. However,

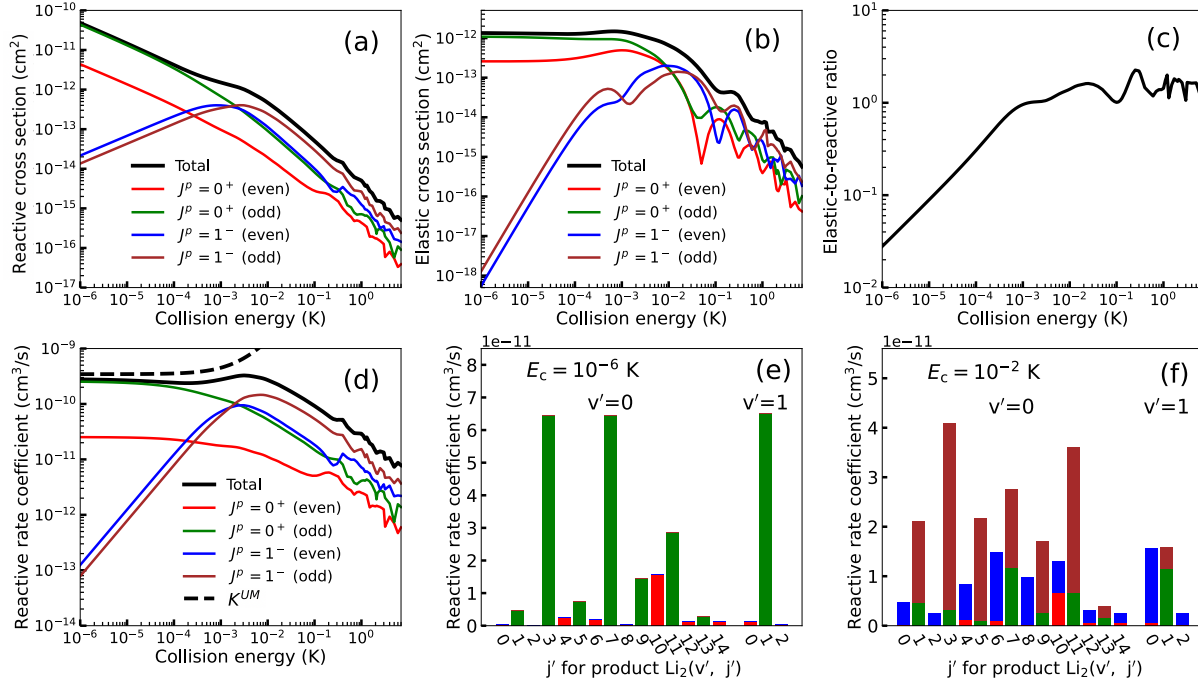


Figure S5: Reactive (a) and elastic (b) cross sections for the ultracold chemical reaction $\text{Li} + \text{NaLi}(v = 0, j = 0) \rightarrow \text{Li}_2 + \text{Na}$ calculated on the pairwise PES (Eq. (S2)) and plotted as a function of collision energy for different values of J , parity p and exchange symmetry. The total integral cross sections (solid black lines) are obtained by summing together the cross sections for even and odd ${}^6\text{Li}$ exchange symmetries multiplied by the statistical factors $1/3$ and $2/3$. We note that these factors are opposite to those used in previous calculations on the ground-state PESs^{S10,S11,S16} because the $X^1\Sigma_g^+$ and $a^3\Sigma_u^+$ electronic states of ${}^6\text{Li}_2$ are even and odd with respect to the exchange of identical Li nuclei. (c) The ratio of elastic to reactive cross sections γ as a function of collision energy. (d) Reaction rate as a function of collision energy. The universal rate is shown by the black dashed line. Nascent product state distributions of Li_2 over final rovibrational states (v', j') at $E = 1 \mu\text{K}$ (e) and $E = 10 \text{ mK}$ (f). The contributions of each J , p , and exchange symmetry are color coded in the same way as in panels (a), (b), and (d).

the numerical agreement of the total reaction rates between the pairwise PES ($\lambda = 0$) and full PES ($\lambda = 1$) is likely the result of a coincidence caused by rapid oscillations in the total rate as a function of λ as shown in Fig. 3(b) in the main text and Figs. S3 and S4. The product state distributions calculated for the pairwise and full PESs are very different as shown in Fig. S5(e). Therefore, despite the coincidental agreement between the $\lambda = 0$ and $\lambda = 1$ total reaction rates, the three-body term provides a significant contribution to short-range reaction dynamics.

Finally, we observe that the total even and odd symmetry rates vary strongly with λ in the vicinity of $\lambda = 1$ differing by as much as a factor of 6. This is similar to the $\lambda = 0$ case, where the odd exchange symmetry contributes almost 10 times more than the even exchange symmetry. While the $\lambda = 0$ case does not correspond to a physical interaction PES, the factor of 10 difference between the even and odd exchange symmetry contributions could constitute an interesting dynamical feature of the pairwise interaction PES, which deserves further study.

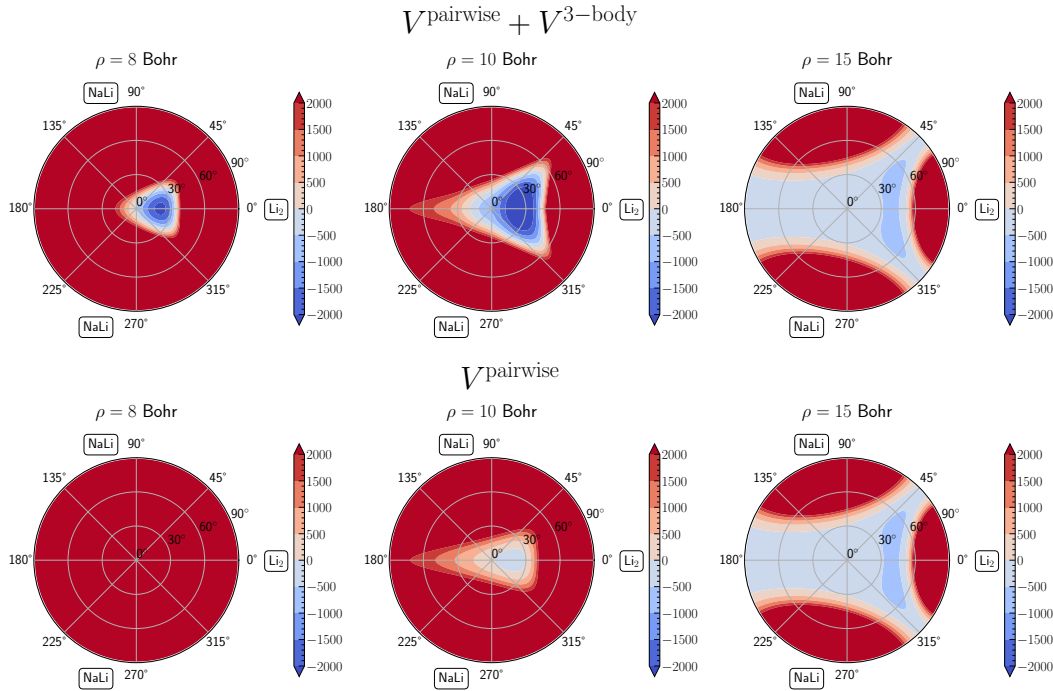


Figure S6: Comparison of the pairwise (bottom panel) and full (top panel) PESs of the NaLi₂ reaction complex.

Figure S5 (e) shows the distributions of Li₂ reaction products over their final rovibrational states (v' , j') at $E = 1 \mu\text{K}$ calculated on the pairwise PES. The contribution from even exchange symmetry with $J^P = 0^+$ (green bars) is dominant, and we observe highly non-uniform distributions in each exchange symmetry, with enhanced reaction rates for the production of Li₂ molecules in the final rovibrational states $j' = 3$ and 7 for $v' = 0$ and $j' = 1$ for $v' = 1$. As shown in panel (f), $J \geq 1$ contributions exceed those from $J = 0$ at $E = 10 \text{ mK}$ for most of the final states. We also observe a decrease in product state selectivity compared to the s -wave limit because the same final rotational states can now be populated in collisions occurring at multiple J and l .

References

- (S1) Werner, H.-J.; *et al.*, MOLPRO, version 2015.1, a package of *ab initio* programs. 2015.
- (S2) Lesiuk, M.; Musiał, M.; Moszynski, R. Potential-energy curve for the $a^3\Sigma_u^+$ state of a lithium dimer with Slater-type orbitals. *Phys. Rev. A* **2020**, *102*, 062806.
- (S3) Hermsmeier, R.; Kłos, J.; Kotochigova, S.; Tscherbul, T. V. Quantum spin state selectivity and magnetic tuning of ultracold chemical reactions of triplet alkali-metal dimers with alkali-metal atoms. *Phys. Rev. Lett.* **2021**, *127*, 103402.
- (S4) Kendrick, B. K.; Li, H.; Li, M.; Kotochigova, S.; Croft, J. F. E.; Balakrishnan, N. Non-

- adiabatic quantum interference in the ultracold $\text{Li} + \text{LiNa} \rightarrow \text{Li}_2 + \text{Na}$ reaction. *Phys. Chem. Chem. Phys.* **2021**, *23*, 5096–5112.
- (S5) Diaz Peña, M.; Pando, C.; Renuncio, J. A. R. Combination rules for three–body van der Waals coefficients. *J. Chem. Phys.* **1980**, *73*, 1750–1756.
- (S6) Axilrod, B. M.; Teller, E. Interaction of the van der Waals Type Between Three Atoms. *J. Chem. Phys.* **1943**, *11*, 299–300.
- (S7) Derevianko, A.; Porsev, S. G.; Babb, J. F. Electric dipole polarizabilities at imaginary frequencies for hydrogen, the alkali–metal, alkaline–earth, and noble gas atoms. *At. Data Nucl. Data Tables* **2010**, *96*, 323–331.
- (S8) Pack, R. T.; Parker, G. A. Quantum reactive scattering in three dimensions using hyperspherical (APH) coordinates. Theory. *J. Chem. Phys.* **1987**, *87*, 3888–3921.
- (S9) Kendrick, B. K.; Pack, R. T.; Walker, R. B.; Hayes, E. F. Hyperspherical surface functions for nonzero total angular momentum. I. Eckart singularities. *J. Chem. Phys.* **1999**, *110*, 6673–6693.
- (S10) Kendrick, B. K. Non-adiabatic quantum reactive scattering in hyperspherical coordinates. *J. Chem. Phys.* **2018**, *148*, 044116.
- (S11) Makrides, C.; Hazra, J.; Pradhan, G. B.; Petrov, A.; Kendrick, B. K.; González-Lezana, T.; Balakrishnan, N.; Kotochigova, S. Ultracold chemistry with alkali-metal–rare-earth molecules. *Phys. Rev. A* **2015**, *91*, 012708.
- (S12) Parker, G. A.; Walker, R. B.; Kendrick, B. K.; T Pack, R. Accurate quantum calculations on three-body collisions in recombination and collision-induced dissociation. I. Converged probabilities for the $\text{H} + \text{Ne}_2$ system. *J. Chem. Phys.* **2002**, *117*, 6083–6102.
- (S13) Idziaszek, Z.; Julienne, P. S. Universal rate constants for reactive collisions of ultracold molecules. *Phys. Rev. Lett.* **2010**, *104*, 113202.
- (S14) Julienne, P. S.; Hanna, T. M.; Idziaszek, Z. Universal ultracold collision rates for polar molecules of two alkali-metal atoms. *Phys. Chem. Chem. Phys.* **2011**, *13*, 19114–19124.
- (S15) Gribakin, G. F.; Flambaum, V. V. Calculation of the scattering length in atomic collisions using the semiclassical approximation. *Phys. Rev. A* **1993**, *48*, 546–553.
- (S16) Kendrick, B. K. Quantum reactive scattering calculations for the cold and ultracold $\text{Li} + \text{LiNa} \rightarrow \text{Li}_2 + \text{Na}$ reaction. *J. Chem. Phys.* **2021**, *154*, 124303.
- (S17) Croft, J. F. E.; Hazra, J.; Balakrishnan, N.; Kendrick, B. K. Symmetry and the geometric phase in ultracold hydrogen-exchange reactions. *J. Chem. Phys.* **2017**, *147*, 074302.